

October 20, 2016

Computational design of PDZ domains: parameterization and performance of a simple model

David Mignon¹, Nicolas Panel¹, Xingyu Chen and Thomas Simonson*

[†]Laboratoire de Biochimie (UMR CNRS 7654), Ecole Polytechnique, Palaiseau, France

¹Joint first authors. *Corresponding author: thomas.simonson@polytechnique.fr

Short title: Computational design of PDZ domains

Keywords:

Abstract

PDZ domains help direct protein-protein interactions and have been extensively studied and engineered. Here, a protein design energy function is optimized for a small set of PDZ domains. It combines a molecular mechanics protein energy, Generalized Born solvent, and an empirical unfolded state model characterized by amino acid type-dependent chemical potentials. These are optimized using a maximum likelihood formalism and several implementation variants. Sequences designed with the best variants are almost all recognized by the Superfamily fold recognition tool and have similarity scores relative to experimental sequences comparable to sequences designed with the Rosetta software and to similarities between natural PDZ domains. Several designs prove stable in 200–500 ns molecular dynamics simulations. The model is then used to redesign the hydrophobic core of two PDZ domains, with the help of a bias potential that alters the chemical potential of hydrophobic amino acid types. By varying the bias, we gradually enrich or deplete the protein in hydrophobic types. The tendency of each position to retain, lose, or gain a hydrophobic character represents a novel, structure-based measure of hydrophobicity, whose mean value differs by a factor of two between the two proteins. In a second application, we redesign four Tiam1 positions involved in peptide binding affinity and specificity, three of which are part of the hydrophobic core. The calculations are done for the apo protein and with two different peptide ligands. The designed sequences are homologous to the wildtype sequence, LKLL, and an experimental quadruple mutant, MEFV, which has different affinities for the two peptides. Experimental affinity differences between protein variants are reproduced qualitatively.

1 Introduction

PDZ domains are small, globular protein domains that help establish protein-protein interaction networks in the cell [1–6]. They form specific interactions with other, target proteins, usually by recognizing a few amino acids at the target C-terminus. Due to their biological importance, PDZ domains and their ligands have been extensively studied and engineered, including many studies with computational methods. Peptide ligands have been designed that modulate the activity of PDZ domains involved in various pathologies [7–9]. Engineered PDZ domains and PDZ ligands have been used to elucidate principles of protein folding and evolution [10–13]. In addition, these small domains with their peptidic ligands provide benchmarks to test the computational methods themselves [14–16].

One emerging method that has been applied to several PDZ domains is computational protein design (CPD) [17–22]. Starting from a 3D structural model, CPD explores a large space of sequences and conformations to identify protein variants that have certain predefined properties, such as stability or ligand binding. Conformational space is usually defined by a library of sidechain rotamers, which can be discrete or continuous, and by a finite set of backbone conformations or a specific repertoire of allowed backbone deformations. The energy function usually combines physical and empirical terms [23–25]. Both solvent and the unfolded protein state are described implicitly.

Here, we consider a simple but important class of CPD variants; we optimize selected parameters of the energy function for a group of PDZ proteins; we test the quality of the model, and we use it for two applications. Our CPD variant is implemented in the Proteus software [26–28]. It uses an “MMGBSA” energy function, which combines a molecular mechanics protein energy with a Generalized Born + Surface Area implicit solvent treatment. The folded protein is represented by a single, fixed, backbone conformation and a discrete sidechain rotamer library. The unfolded state energy depends only on sequence composition, not an explicit structural model. With this CPD variant, the main adjustable model parameters are the protein dielectric constant ϵ_P , a small set of atomic surface energy coefficients σ_i , and a collection of amino acid chemical potentials, or “reference energies” E_t^r that each represent the contribution of a single amino acid of type t to the unfolded state energy.

We optimize the reference energies E_t^r using a maximum likelihood formalism and a set of eight PDZ test proteins. For two of the proteins, Tiam1 and Cask, we compare two sets of surface coefficients and two values of the dielectric constant. The resulting

parameter sets are tested by generating designed sequences for all eight proteins and comparing them to natural sequences, as well as sequences generated with the Rosetta energy function and software [29]. We also perform 100-500 nanosecond molecular dynamics simulations for a few designed sequences, to help assess their stability.

We then apply the optimized model to the Tiam1 protein and two problems. First, we do a series of Monte Carlo simulations of Tiam1 where the chemical potential of the hydrophobic amino acid types is gradually increased, artificially biasing the protein composition. As we increase the bias, hydrophobic amino acids gradually invade the protein interior, forming a hydrophobic core that is initially smaller, then becomes larger than the natural one. The propensity of each core position to become hydrophobic at a high or low level of bias can be seen as a structure-dependent hydrophobicity index, providing information on the designability of the protein core. The second application consists in designing four Tiam1 positions that are known to be involved in specific target recognition, and have been experimentally mutated so as to modify the preferred Tiam1 target [30], increasing its preference for the Caspr4 peptide, with respect to the syndecan-1 peptide (Sdc1). We mutate these positions through Monte Carlo simulations of either the apo-protein or the protein in complex with either peptide ligand.

2 The unfolded state model

2.1 Maximum likelihood reference energies

We use Monte Carlo to generate a Markov chain of states [31, 32], such that the states are populated according to a Boltzmann distribution. One possible elementary move is a “mutation”: we modify the sidechain type $t \rightarrow t'$ at a chosen position i in the folded protein, assigning a particular rotamer r' to the new sidechain. At the same time, we perform the reverse mutation in the unfolded protein, $t' \rightarrow t$. For a particular sequence S , the unfolded state energy has the form:

$$E_S^u = \sum_{i \in S} E^r(t_i). \quad (1)$$

The sum is over all amino acids; t_i represents the sidechain type at position i . The type-dependent quantities $E^r(t) \equiv E_t^r$ are referred to as “reference energies”. The energy change due to a mutation has the form:

$$\Delta E = \Delta E^f - \Delta E^u = (E^f(\dots t'_i, r'_i \dots) - E^f(\dots t_i, r_i \dots)) - (E^r(t'_i) - E^r(t_i)) \quad (2)$$

The reference energies are essential parameters in the simulation model. Our goal here is to choose them empirically so that the simulation produces amino acid frequencies that match a set of target values, for example experimental values in the Pfam database. Specifically, we will choose them so as to maximize the probability, or likelihood of the target sequences.

Let S be a particular sequence. Its Boltzmann probability is

$$p(S) = \frac{1}{Z} \exp(-\beta \Delta G_S), \quad (3)$$

where $\Delta G_S = G_S^f - E_S^u$ is the folding free energy of S , G_S^f is the free energy of the folded form, $\beta = 1/kT$ is the inverse temperature and Z is a normalizing constant (the partition function). We then have

$$kT \ln p(S) = \sum_{i \in S} E^r(t_i) - G_S^f - kT \ln Z = \sum_{t \in aa} n_S(t) E_t^r - G_S^f - kT \ln Z, \quad (4)$$

where the sum on the right is over the amino acid types and $n_S(t)$ is the number of amino acids of type t within the sequence S .

We now consider a set \mathcal{S} of N target sequences S ; we denote \mathcal{L} the probability of the entire set, which depends on the model parameters E_t^r ; we refer to \mathcal{L} as their likelihood [33]. We have

$$kT \ln \mathcal{L} = \sum_S \sum_{t \in aa} n_S(t) E_t^r - \sum_S G_S^f - N kT \ln Z = \sum_{t \in aa} N(t) E_t^r - \sum_S G_S^f - N kT \ln Z, \quad (5)$$

where $N(t)$ is the number of amino acids of type t in the whole dataset \mathcal{S} . The normalization factor or partition function Z is a sum over all possible sequences R :

$$Z = \sum_R \exp(-\beta \Delta G_R) = \sum_R \exp(-\beta \Delta G_R^f) \prod_{s \in aa} \exp(\beta n_R(s) E_s^r) \quad (6)$$

In view of maximizing \mathcal{L} , we consider the derivative of Z with respect to one of the E_t^r :

$$\frac{\partial Z}{\partial E_t^r} = \sum_R \beta n_R(t) \exp(-\beta \Delta G_R^f) \prod_{s \in aa} \exp(\beta n_R(s) E_s^r) \quad (7)$$

We then have

$$\frac{kT}{Z} \frac{\partial Z}{\partial E_t^r} = \frac{\sum_R n_R(t) \exp(-\beta \Delta G_R)}{\sum_R \exp(-\beta \Delta G_R)} = \langle n(t) \rangle. \quad (8)$$

The quantity on the right is the Boltzmann average of the number $n(t)$ of amino acids t over all possible sequences. In practice, this is the average population of t we would

obtain in a long MC simulation. We note that, as usual in statistical mechanics [34], the derivative of $\ln Z$ with respect to one quantity (E_t^r) is equal to the ensemble average of the conjugate quantity ($\beta n_S(t)$).

A necessary condition to maximize $\ln \mathcal{L}$ is that its derivatives with respect to the E_t^r should all be zero. We see that

$$\frac{1}{N} \frac{\partial}{\partial E_t^r} \ln \mathcal{L} = \frac{1}{N} \sum_S n_S(t) - \langle n(t) \rangle = \frac{N(t)}{N} - \langle n(t) \rangle \quad (9)$$

so that

$$\mathcal{L} \text{ maximum} \implies \frac{N(t)}{N} = \langle n(t) \rangle, \quad \forall t \in \text{aa} \quad (10)$$

Thus, to maximize \mathcal{L} , we should choose $\{E_t^r\}$ such that a long simulation gives the same amino acid frequencies as the target database.

2.2 Searching for the maximum likelihood

To approach the maximum likelihood $\{E_t^r\}$ values, starting from a current guess $\{E_t^r(n)\}$, we will use two methods. With the first method, we step along the gradient of $\ln \mathcal{L}$, using the update rule [33]:

$$E_t^r(n+1) = E_t^r(n) + \alpha \frac{\partial}{\partial E_t^r} \ln \mathcal{L} = E_t^r(n) + \delta E (n_t^{\text{exp}} - \langle n(t) \rangle_n) \quad (11)$$

Here, α is a constant; $n_t^{\text{exp}} = N(t)/N$ is the mean population of amino acid type t in the target database; $\langle \cdot \rangle_n$ indicates an average over a simulation done using the current reference energies $\{E_t^r(n)\}$, and δE is an empirical constant with the dimension of an energy, referred to as the update amplitude. This update procedure is repeated until convergence. We refer to this method as the linear update method.

The second method, used previously [26, 27], employs a logarithmic update rule:

$$E_t^r(n+1) = E_t^r(n) + kT \ln \frac{\langle n(t) \rangle_n}{n_t^{\text{exp}}} \quad (12)$$

where kT is a thermal energy, set empirically to 0.5 kcal/mol. We refer to this as the logarithmic update method. Both the linear and logarithmic update methods converge to the same optimum, specified by (Eq. 10).

In the later iterations, some E_t^r values tended to converge slowly, with an oscillatory behavior. Therefore, we sometimes used a modified update rule, where the $E_t^r(n+1) -$

$E_t^r(n)$ value computed with the linear or logarithmic method for iteration n was mixed with the value computed at the previous iteration, with the $(n - 1)$ value having a weight of $1/3$ and the current value a weight of $2/3$. At each iteration, we typically ran 500 million steps (per replica) of Replica Exchange Monte Carlo.

3 Computational methods

3.1 Effective energy function for the folded state

The energy matrix was computed with the following effective energy function for the folded state:

$$E = E_{\text{bonds}} + E_{\text{angles}} + E_{\text{dihedral}} + E_{\text{impr}} + E_{\text{vdw}} + E_{\text{Coul}} + E_{\text{solv}} \quad (13)$$

The first six terms in (13) represent the protein internal energy. They were taken from the Amber ff99SB empirical energy function [35], slightly modified for CPD (see below). The last term on the right, E_{solv} , represents the contribution of solvent. We used a “Generalized Born + Surface Area”, or GBSA implicit solvent model [36]:

$$E_{\text{solv}} = E_{\text{GB}} + E_{\text{surf}} = \frac{1}{2} \left(\frac{1}{\epsilon_W} - \frac{1}{\epsilon_P} \right) \sum_{ij} q_i q_j (r_{ij}^2 + b_i b_j \exp[-r_{ij}^2/4b_i b_j])^{-1/2} + \sum_i \sigma_i A_i \quad (14)$$

Here, ϵ_W , ϵ_P are the solvent and protein dielectric constants; r_{ij} is the distance between atoms i, j and b_i is the “solvation radius” of atom i [36, 37]. A_i is the exposed solvent accessible surface area of atom i ; σ_i is a parameter that reflects each atom’s preference to be exposed or hidden from solvent. The solute atoms were divided into 4 groups with specific σ_i values (see below): unpolar, aromatic, polar, and ionic. Hydrogen atoms were assigned a surface coefficient of 0. Surface areas were computed by the Lee and Richards algorithm [38], implemented in the XPLOR program [39], using a 1.5 Å probe radius. Most of the MC simulations used a protein dielectric of $\epsilon_P = 4$ or 8 (see Results).

In the GB energy term, the atomic solvation radius b_i approximates the distance from i to the protein surface and is a function of the coordinates of all the protein atoms. The particular b_i form corresponds to a GB variant we call GB/HCT, after its original authors [36], with model parameters optimized for use with the Amber force field [37]. Since b_i depends on the coordinates of all the solute atoms [36], an additional approximation is needed to make the GB energy term pairwise additive and define the energy matrix. We

use a “Native Environment Approximation”, or NEA, where the solvation radius b_i of each particular group (backbone, sidechain or ligand) is computed ahead of time, with the rest of the system having its native sequence and conformation [27, 40].

The surface energy contribution E_{surf} is not pairwise additive either, because in a protein structure, surface area buried by one sidechain may also be buried by another. To make this energy pairwise, Street et al proposed a simple procedure [41]. The buried surface of a sidechain is computed by summing over the neighboring sidechain and backbone groups. For each neighboring group, the contact area with the sidechain of interest is computed, independently of other surrounding groups. The contact areas are then summed. To avoid overcounting of buried surface area, a scaling factor is applied to the contact areas involving buried sidechains. Previous work showed that a scaling factor of 0.65 works well [37, 40].

The Amber force field ff99SB is slightly modified for CPD, with the original backbone charges replaced by a unified set, obtained by averaging over all amino acid types and adjusting slightly to make the backbone portion of each amino acid neutral [42].

3.2 Reference energies in the unfolded state

In the unfolded state, the energy depends on the sequence composition through a set of reference energies E_t^r (Eq. 1). The values are assigned based on amino acid types t , taking into account also the position of each amino acid in the folded structure, through its buried or solvent-exposed character. Thus, for a given type (Ala, say), there are two distinct E_t^r values: a buried and an exposed value. This is done even though the reference energies are used to represent the unfolded, not the folded state. There are three rationales for this. First, we assume residual structure is present in the unfolded state, so that amino acids partly retain their buried/exposed character. Second, we hypothesize that the unfolded state model compensates in a systematic way for errors in the folded state energy function, so that the folded structure matters. Third, this strategy makes the model less sensitive to variations in the length of surface loops, and to the proportion of surface vs. buried residues, which can vary widely among homologs (see below); as a result, the model should be more transferable within a protein family.

Distinguishing buried/exposed positions doubles the number of adjustable E_t^r parameters. Conversely, to reduce the number of adjustable parameters, we group amino acids into homologous classes (given in Results). Within each class c , and for each type

of position (buried or exposed), the reference energies have the form

$$E_t^r = E_c^r + \delta E_t^r \quad (15)$$

Here, E_c^r is an adjustable parameter while δE_t^r is a constant, computed as the molecular mechanics energy difference between amino acid types within the class c , assuming an unfolded conformation where each amino acid interacts only with itself and with solvent. During likelihood maximization, E_c^r is optimized while δE_t^r is held fixed. To optimize the E_c^r values, we apply the linear or logarithmic method above; the target frequencies correspond to the experimental frequencies of the amino acid classes, n_c^{exp} , rather than of the individual types (n_t^{exp} , above).

3.3 Experimental sequences

We considered a set of eight PDZ domains, whose PDB codes are listed in Table 1. To define the target amino acid frequencies for likelihood maximization, we collected homologous sequences for each of the eight. We started by a Blast search of the Uniprot database with the PDB sequence as the query, using the Blosum62 matrix, and retained homologs with a sequence identity, relative to the query, above a certain threshold, around 60–80% depending on the test protein. Sequences that were over 95% or 85% identical to the query were removed, and homologs with mutual identities above 95% were pruned, keeping just one of the redundant variants. This led to about 40–120 homologs per test protein; see details in Table 1. For each set, amino acid frequencies were computed, distinguishing buried and exposed positions. Buried positions were defined to have a solvent-accessible surface area below 30% of that obtained for the amino acid alone, which led to similar numbers of buried/exposed positions. The eight sets of mean frequencies were themselves averaged, giving the overall target amino acid frequencies (see below).

3.4 Structural models

Structures were prepared and energy matrices computed using procedures described previously [15, 43]. For Tiam1, two missing segments (residues 851–854 and 868–869) were built using the Modeller program [44]. In the energy matrix calculations, for each residue pair, interaction energies were computed after 15 steps of energy minimization, with the backbone fixed and only the interactions of the pair with each other and the backbone

included. This short minimization of pairs alleviates the discrete rotamer approximation. Sidechain rotamers were described by a slightly expanded version of the library of Tuffery et al [45], which has a total of 254 rotamers (sum over all amino acid types). The expansion consists in allowing additional hydrogen orientations for OH and SH groups [40]. This rotamer library was chosen for its simplicity and because it gives very good performance in sidechain placement tests, comparable to the specialized Scwrl4 program (which uses a much larger library) [46, 47].

3.5 Monte Carlo simulations

The Monte Carlo simulations used one- and two-position moves, where either rotamers, types, or both are changed. For two-position moves, the second position is selected among those that have a significant (unsigned) interaction energy with the first one, meaning that there is at least one rotamer conformation where their interaction is 10 kcal/mol or more. In addition, we mostly perform Replica Exchange Monte Carlo (REMC), where several simulations (“replicas” or “walkers”) are propagated in parallel, at different temperatures; periodic swaps are attempted between the conformations of two walkers i, j (adjacent in temperature). The swap is accepted with probability

$$acc(\text{swap}_{ij}) = \text{Min} \left[1, e^{(\beta_i - \beta_j)(\Delta E_i - \Delta E_j)} \right] \quad (16)$$

where β_i, β_j are the inverse temperatures of the two walkers and $\Delta E_i, \Delta E_j$ are the changes in their folding energies due to the conformation change [48, 49]. We use eight walkers, with thermal energies kT_i that range from 0.125 to 2 kcal/mol, and are spaced in a geometric progression: $T_{i+1}/T_i = \text{constant}$ [48]. Simulations are done with the proteus program [27]; REMC uses an efficient, shared-memory, OpenMP parallelization [50].

For the Tiam1 protein, a few simulations were also done that included a biasing potential, which penalizes sequences with a low similarity to a reference, experimental set. The bias energy had the form

$$\delta E_{\text{bias}} = c \sum_i (S(t_i) - S_i^{\text{rand}}), \quad (17)$$

where the sum is over the amino acid positions i , t_i is the sidechain type at position i , $S(t_i)$ is the (dimensionless) Blosum40 similarity score versus the corresponding position in the Pfam RP55 sequence alignment; S_i^{rand} is the mean score (versus the same Pfam column) for a random type (where all types are equiprobable), and $c = 1$ kcal/mol.

3.6 Rosetta sequence generation

Monte Carlo simulations were also done using the Rosetta program and energy function [29]. The simulations were done using version 2015.38.58158 of Rosetta (freely available online), using the command

```
fixbb -s Tiam1.pdb -resfile Tiam1.res -nstruct 10000 -ex1 -ex2 -linmem_ig 10
```

which corresponds to default parameters. Simulations were run for each protein until 10000 low energy sequences were identified, corresponding to run times of about 5 minutes per sequence on a single core of a recent Intel processor, for a total of 10 hours (per protein) using 80 cores. This is comparable to the cost of the Proteus calculations (energy matrix plus Monte Carlo).

3.7 Sequence characterization

Designed sequences were compared to the Pfam alignment for the PDZ family, using the Blosum40 scoring matrix and a gap penalty of -6. Each Pfam sequence was also compared to the Pfam alignment. For these Pfam/Pfam comparisons, if a test protein T was part of the Pfam alignment, the T/T self comparison was left out, to be more consistent with the designed/Pfam comparisons. The Pfam alignment was the “RP55” alignment, with 12255 sequences. Similarities were computed for 14 core residues and 16 surface residues, defined by their near-complete burial or exposure (listed in Results) and for the entire protein.

Designed sequences were submitted to the Superfamily library of Hidden Markov Models [51, 52], which attempts to classify sequences according to the SCOP classification [53]. Classification was based on SCOP version 1.75 and version 3.5 of the Superfamily tools. Superfamily executes the hmmscan program, which implements a Hidden Markov model for each SCOP family and superfamily; here hmmscan was executed with an E-value threshold of 10^{-10} , using a total of 15438 models to represent the SCOP database.

To compare the diversity in the designed sequences with the diversity in natural sequences, we used a standard, position-dependent sequence entropy [54], computed as follows:

$$S_i = - \sum_{j=1}^6 f_j(i) \ln f_j(i) \quad (18)$$

where $f_j(i)$ is the frequency of residue type j at position i , either in the designed sequences or in the natural sequences (organized into a multiple alignment). Instead of the

usual, 20 amino acid types, we employ six residue classes, corresponding to the following groups: {LVIMC}, {FYW}, {G}, {ASTP}, {EDNQ}, and {KRH}. This classification was obtained by a cluster analysis of the BLOSUM62 matrix [55], and also by analyzing residue-residue contact energies in proteins [56]. To get a sense of how many amino acid types appear at a specific position i , we report the residue entropy in its exponentiated form, $\exp(S_i)$ (which ranges from 1 to 6), averaged over the protein chain (i.e., S_i is exponentiated first, then averaged over positions).

3.8 Molecular dynamics simulations

For wildtype Tiam1 and a few designed sequences, we ran MD simulations with explicit solvent. Starting structures were taken from the MC trajectory or the crystal structure (wildtype protein) and slightly minimized through 200 steps of conjugate gradient minimization. The protein was immersed in a large box of water; waters overlapping protein were eliminated, and the solvated system was truncated to the shape of a truncated octahedral box using the Charmm graphical interface or GUI [57]; the minimum distance between protein atoms and the box was 15 Å; final models included about 11000 water molecules. A few sodium or chloride ions were included to ensure overall electroneutrality. Protonation states of histidines were assigned to be neutral, based on visual inspection. MD was done at room temperature and pressure, using a Nose-Hoover thermostat and barostat. Long-range electrostatic interactions were treated with a Particle Mesh Ewald approach [58]. The Amber ff99SB forcefield was used for the protein; the TIP3P model [59] was used for water. Simulations were run for 100–500 nanoseconds, depending on the sequence, using the Charmm and NAMD programs [60, 61].

4 Results

4.1 Experimental structures and sequences

We begin by a brief overview of the test proteins. 3D structures are shown in Fig. 1A; for clarity, only four of the eight proteins are shown. 14 core residues (highlighted by their C_β atoms, shown as spheres) superimpose well between structures; loops and chain termini display large deviations, and the Tiam1 α_2 helix is rotated slightly outwards compared to the other three structures. Fig. 1B illustrates the similarity between all eight domains, measured by the rms deviation between structurally-aligned C_α atoms. Structure pairs

with rms deviations of 1 Å or less and 60 aligned residues or more are linked; 2BYG forms the center of the group, with five links; Cask is not quite linked to 1IHJ (rms deviation of 1.3 Å over 63 residues) and Tiam1 is isolated. Sequence identities are also shown, including those between Tiam1 and its closest homologs. Overall, six proteins form a tight group, with deviations of 1 Å or less, while Cask and Tiam1 are further away. The Tiam1/Cask sequence identity is 33%; their structural deviation is 1.7 Å based on a 42-residue alignment.

Sequence conservation within our eight proteins and a subset of the Pfam seed alignment (half) is shown in Fig. 2. The 14 positions we use to define the hydrophobic core are highly, though not totally conserved within the Pfam seed alignment. Arg, Lys and Gln appear at some of the positions, since in a small PDZ protein, the long hydrophobic portion of these sidechains can be buried in the core while still allowing the polar tip of the sidechain to be exposed to solvent. Small amounts of Asp, and Glu also appear, in places where the sequence alignment may not reflect closely the 3D sidechain superposition (or lack thereof).

4.2 Optimizing the unfolded state model

We optimized the reference energies E_t^r for six of the eight proteins, with the other two (Tiam1, Cask) left for cross validation. The protein dielectric constant was $\epsilon_P = 8$, and a first set of atomic surface coefficients was used. We refer to the resulting model either as model A or as the ($\epsilon_P=8$, S1, $n=6$) model (S1 for “set 1”; $n=6$ represents the number of proteins used to define the target amino acid frequencies). We repeated the optimization for Tiam1 and Cask alone, to see what improvement is obtained, if any, when a smaller set of proteins is specifically optimized. The resulting model is called A' or ($\epsilon_P=8$, S1, $n=2$). Finally, we repeated the E_t^r optimization using a second set of surface coefficients and an ϵ_P of either 8 or 4; these calculations were done for Tiam1 and Cask alone, due to the cost of repeated optimizations with multiple proteins. The corresponding models are called B ($\epsilon_P=8$, S2, $n=2$) and B' ($\epsilon_P=4$, S2, $n=2$). Model names are listed in Table 2. The optimizations all converged to within 0.05 kcal/mol after about 20 iterations for most amino acid types, and within 0.1 kcal/mol for the others (the weakly-populated types), using either the linear or the logarithmic method. Table 3 indicates the final reference energies for models A and B, which give the best performance (see below). The E_t^r values are compared to, and agree qualitatively with the energies computed from an extended peptide structure, which provides a less empirical model of the unfolded state. Table

4 compares the amino acid frequencies from experiment and the simulations. We see that while the theoretical populations of the different amino acid classes agree well with experiment, the agreement for some of the amino acid types is not perfect. The intra-class frequency distributions depend explicitly on the energy offsets δE_t^r defined within each class, which are computed with molecular mechanics (see Methods).

4.3 Assessing designed sequence quality

Family recognition tests Proteus simulations used Replica Exchange Monte Carlo (REMC) with eight replicas at temperatures between 0.236 and 3 kcal/mol; 750 million steps (per replica) were run; the 10000 lowest energies among those sampled by any of the the replicas were retained for analysis, along with the 10000 Rosetta sequences. These sequences were submitted to the Superfamily fold recognition tool. Results are given in Table 5. For 6 of 8 proteins, all 10000 Rosetta sequences are assigned by Superfamily to the correct SCOP superfamily and family, with E-values between $0.5 \cdot 10^{-3}$ and $4 \cdot 10^{-3}$ for the family assignments. For two, the family success rates are 90/98%, with slightly higher E-values. With model A = ($\epsilon=8, S1, n=6$), the Proteus results are also good, with 6 out of 8 proteins giving 100% of correct family assignments, with E-values between $2 \cdot 10^{-3}$ and $15 \cdot 10^{-3}$ for the family assignments. For the 1R6J and Tiam1 proteins, only 13% and 4 %, respectively, of the top sequences were assigned to the correct family. For these two proteins, with the Proteus sequences, Superfamily only recognizes about half of the sequence length; for the other 6 proteins, the Superfamily match lengths are similar to those seen with the Rosetta sequences. Notice that Tiam1 was not part of the reference energy optimization set (nor was Cask). Specifically optimizing the reference energies for Tiam1 and Cask (model A') did not improve the Superfamily performance, with just 0.1% of correct family assignments for Tiam1 and 63% for Cask (vs. 4% and 100% with model A).

Switching to a second set of surface coefficients (model B) gave significantly improved Proteus results for Tiam1 and Cask, even though these values (set 2) were optimized earlier using a *different* solvent model (Coulombic instead of Generalized Born electrostatics) [62]. Using these coefficients and E_t^r values optimized for Tiam1 and Cask (model B or $\epsilon=8, S2, n=2$), we obtained a high percentage of sequences assigned to the correct family: 91% for Tiam1 and 100% for Cask, slightly better than Rosetta. Changing the protein dielectric constant to $\epsilon_P=4$ (model B') gave results for Tiam1 that were somewhat poorer than model B but still much better than model A.

Sequences and sequence diversity Tiam1 and Cask sequences predicted by Proteus, using model B, and by Rosetta are shown as sequence logos, both for the 14 core residues (Fig. 3) and for 16 surface residues (Tiam1 only; Fig. 4), and compared to natural sequences. Agreement with experiment for the core residues is very good, while agreement for the surface residues is much poorer, as seen in many previous CPD studies. The behavior of the surface positions is also illustrated by designing each position individually, with the rest of the protein free to explore rotamers but not mutations (“single-position” design). The corresponding logo shows an excess of Arg and Lys residues, suggesting that their model B reference energies are not yet optimal, despite the extensive empirical E_t^r tuning. Sequence similarity scores are given in the next subsection.

The diversity of the natural and designed sequences can be characterized by a mean, exponentiated sequence entropy (see Methods), which corresponds to a mean number of sampled sequence classes per position. The large, RP55 set of experimental sequences has a mean entropy of 3.4. Pooling the designed Tiam1 and Cask sequences gives an entropy of 2.2 with Rosetta and 2.2 with Proteus and model A, or 2.0 with model B, indicating that these two backbone geometries cannot accomodate as much diversity as the much larger RP55 set. Taking the 10000 lowest energy sequences sampled with the *room temperature* Monte Carlo replica (instead of the 10000 lowest energies sampled by all replicas) and pooling Tiam1 and Cask as before gives a higher overall entropy of 3.0/2.9 with Proteus models A/B. Entropy in the core is only slightly below average (2.1 and 2.0) with Rosetta and model A, but only 1.25 with Proteus model B, compared to 1.8 for Pfam-RP55.

Blosum similarity scores We also computed Blosum40 similarity scores between designed and experimental sequences, shown in Figs. 5 and 6. With model A = ($\epsilon=8, S1, n=6$), for the 14 core residues, the scores for all but one protein overlap with the scores seen within the RP55 set of experimental sequences, with values between 20 and 40 (Fig. 5). The 1R6J protein, which gave low Superfamily scores, does well in terms of Blosum40 scores. Only for 3K82 are the Proteus scores in the very low range of the experimental scores. Rosetta does somewhat better for this protein. For the seven others, results for the Rosetta sequences are similar on average to Proteus, with some cases a bit better and others a bit worse. The Proteus sequences for Tiam1 and Cask score mostly above the Rosetta sequences, even though these proteins were not part of model A’s E_r^t optimization set.

With model B = ($\epsilon=8, S2, n=2$), the Cask results are similar to model A and the Tiam1 results slightly improved (whereas the Superfamily results were greatly improved). With model B, we also computed surface and overall similarities (Fig. 6). The overall similarities overlap with the bottom of the peak of experimental scores, and are comparable to the values for the Rosetta sequences. For the surface residues, similarity to the experimental sequences is low (scores below zero), both for Proteus and Rosetta. Model B' (not shown) performs about as well as model B, giving the same similarity averaged over all Tiam1 and Cask positions, for example.

While the similarity scores vs. Pfam with our models are comparable to Rosetta, the identity scores vs. the wildtype sequence are significantly higher with Rosetta: 27 \pm 6% for model A and xxx% with model B vs. 41 \pm 9% for Rosetta (excluding Gly and Pro positions, which do not mutate).

For certain applications, we may need to specifically explore a sequence space region that is very similar to Pfam, beyond the similarity that is provided by an approximate energy function such as the MMGBSA one. This can be achieved by adding to the energy function an umbrella potential that explicitly favors high sequence scores. Fig. 6 includes results that use such a bias potential (see Methods): by construction, it leads to very high (and tunable) similarity scores, above the mean similarity between Pfam sequences in this particular case.

We also analyzed the similarity between theoretical sequences generated with the different Proteus models. With model B, overall similarity scores between the Proteus sequences (model B vs. itself) are 453 \pm 22 for Tiam1 and 491 \pm 20 for Cask. Changing the dielectric constant to 4 (model B') gives sequences less similar to model B, with B-B' scores of 389 \pm 18 and 412 \pm 30 for Tiam1 and Cask, respectively. Changing the surface coefficients to set 1 (model A) changes the sequences more substantially, with A-B scores of 173 \pm 11 and 150 \pm 14 for Tiam1 and Cask, respectively.

4.4 Stability of designed sequences in molecular dynamics simulations

Ten designed Tiam1 sequences were chosen for testing in molecular dynamics simulations with an explicit solvent environment. The sequences were produced using the best design models, B and B' ($\epsilon_P=8/4, S2, n=2$). Among the 2500 lowest energy sequences, we chose ones that had a nonneutral isoelectric point, that were assigned to the correct SCOP

family by Superfamily with good E-values, that had good Pfam similarity scores, and not too many mutations that drastically change the amino acid type compared to the wildtype protein. This left us with 66 sequences from model B and 45 from model B'. In addition, we eliminated two mutations that created a buried cavity and several that led to net protein charges of +6 or more. Six sequences were chosen; four were modified further by hand to eliminate charged residues in the exposed loop 852–856 (lysines changed manually to alanine), for a final set of ten sequences. Simulations were run for 100 ns, then extended to 200 ns for the cases that did not exhibit instability within 100 ns (five sequences; Fig. 7). Three of the five were stable after 200 ns; one was extended to 500 ns and remained stable; we call it “sequence 6”. The native Tiam1 protein was also simulated for 500 ns and remained stable. The experimental Tiam1 stability is weak, with an unfolding free energy of about 3 kcal/mol (E. Fuentes, personal communication). While 200-500 ns simulation times are still short compared to experimental unfolding times (microseconds), they are long enough to challenge the structural models, in the context of a high quality protein force field and an explicit solvent environment. Some of the sequences rapidly drifted away from the starting, designed structure, as measured by their rms deviation (Fig. 7), suggesting they may be unstable or weakly stable. Two moved a few Ångstroms away from the starting, designed structure then stayed put over 200 ns, suggesting a higher stability. Two sequences appear highly stable, with a structure that is very close to the initial, designed model and to the native Tiam1 structure. This includes sequence 6, which stays within 2 Å of the wildtype structure over 500 ns, similar to the wildtype simulation. The mean sequence-6 MD structure is actually closer to the wildtype experimental structure than the mean wildtype MD structure (rms deviations of 1.2 and 1.5 Å, respectively). In the wildtype simulation, in the absence of a peptide ligand, helix α_2 shifts into the ligand binding pocket part of the time (Fig. 7).

4.5 Application to Tiam1: growing the hydrophobic core

As an application of our optimized models, we examined the designability of the Tiam1 and 2BYG hydrophobic cores. We submitted each protein to Replica Exchange Monte Carlo simulations with a succession of slightly different energy functions, which increasingly favor hydrophobic residues. The first simulation includes a bias energy $\delta = 0.4$ kcal/mol (per position) that *penalizes* hydrophobic amino acid types (ILMVAWFY). The last simulation includes a bias energy $\delta = -0.4$ kcal/mol (per position) that *favors* hydrophobic types by the same amount. Intermediate bias values $\delta = 0.2, 0$, and -0.2

kcal/mol were also simulated. Results are illustrated in Fig. 8 (Tiam1 only). With the largest δ value, the Tiam1 hydrophobic core is depleted, with 17 positions changed to polar types (out of 94); these positions mostly lie on the outer edge of the core. With the intermediate values, the hydrophobic core is native-like. With the most negative δ value, the hydrophobic core has expanded outwards into surface regions, with 17 initially polar positions changed to hydrophobic types. Thus, the mutation numbers are symmetric (± 17 changes), like the bias. Half the changes are in loops and half in secondary structure elements. The observed propensities of each position to become polar or hydrophobic in the presence of a large or small penalty δ can be thought of as a hydrophobic designability measure. Thus, 12 of the 14 conserved core positions (all but 884 and 903) remain hydrophobic even at the highest level of polar bias, along with 22 other positions, indicating that these positions have the highest hydrophobic propensity. Taking the number $\delta N = 34$ of nonpolar \rightarrow polar changes from the lowest to the highest bias, dividing by the bias energy change $\delta E = 0.8$ kcal/mol and by the mean number $N = 52$ of nonpolar positions at zero bias, we obtain the relative number of type changes per unit bias energy, $\frac{1}{N} \frac{\delta N}{\delta E} = 0.84$ changes (per position) per kcal/mol. This quantity can be thought of as an overall hydrophobic designability or susceptibility. For 2BYG, we obtain a much lower value of 0.36 changes per kcal/mol, roughly half the Tiam1 value. While 15 positions change to polar under the strongest polar bias, only 3 change to nonpolar under the strongest nonpolar bias. Thus, the protein’s response is dissymmetric with respect to the bias sign, with a stronger response (or susceptibility) in the polar direction and a much weaker one in the nonpolar direction. It is as if the protein is saturated with nonpolar sidechains and has difficulty accepting more.

4.6 Application to Tiam1: designing specificity positions

As a second application, we have redesigned four positions in Tiam1 that are known to contribute to its specific peptide binding. These positions were engineered experimentally to alter Tiam1 specificity, leading to a quadruple mutant that preferentially binds the Caspr4 peptide instead of the syndecan-1 (Sdc1) peptide [30]. The mutations were L911M, K912E, L915F, L920V. All single and two double mutants were also characterized experimentally. We denote the native sequence LKVV, the quadruple mutant MEFV, and similarly for other variants. All four positions but Lys912 are part of the conserved hydrophobic core. We did REMC simulations where all four positions could mutate simultaneously, in the absence of a peptide ligand, and in the presence of either the Sdc1

or the Caspr4 peptide. We used Proteus model $B' = (\epsilon_P=4, S2, n=2)$, which gave similarity scores (above) equivalent to model B but has a reduced tendency to bury polar sidechains, thanks to its lower dielectric constant. The CPD model was constructed either using either the wildtype or the quadruple mutant crystal structure for the backbone (PDB codes 4GVD and 4NXQ, respectively), shown in Fig. 9. The two structures were determined with the Sdc1 and Caspr4 ligands, respectively. The backbone rms deviation between them is 0.9 Å; the main differences are in the flexible 850–857 loop near the peptide C-terminus and in helix α_2 , pushed slightly outwards in the mutant complex, to accommodate Phe at protein position 915 and at the peptide C-terminus (position 0: peptide positions are numbered backwards from its C-terminus, as is common for PDZ ligands). We expect that the mutant backbone model will better describe variants with Phe at position 915 and the wildtype backbone model will better describe variants with a smaller 915 sidechain.

Results are shown in Fig. 9 as sequence logos. For all systems, we sample native or native-like amino acid types at all positions, whether we use the wildtype or mutant backbone structure. For example, using the wildtype backbone structure (4GVD), Leu911 is preserved in the apo simulations and changed to Ile or Val in the holo simulations; using the mutant backbone structure (4NXQ), the holo simulations sample Ile, Leu and Met. With the mutant backbone, the holo simulations sample somewhat different types at position 911 (Trp, Arg, Lys); all these types appear in low amounts at the corresponding position in the Pfam seed alignment. All the simulations sample mostly Arg, Lys, Gln and occasionally Glu at position 912, and mostly Leu and Val at position 920, similar to the experimental types. Not surprisingly, agreement with the wildtype sequence is better when we use the wildtype Xray structure; agreement with the mutant sequence is better when we use the mutant Xray structure.

Recovery of the precise native and quadruple mutant sequences in the different states (apo, holo) is qualitative, not quantitative. Thus, using the wildtype backbone structure and in the apo state, the room temperature Monte Carlo replica recovers the wildtype sequence LKLL just 2 kcal/mol above the best sequence; the close homolog LKML is the second best sequence overall, and the homologs IKLL and LKLV are just 1–2 kcal/mol higher. The mutant sequence MEFV does not appear, nor do any close homologs, because there is not space for a Phe sidechain at position 915 with this backbone. With the Sdc1 ligand, results are very similar, with MEFV unsampled and LKLL, IKLL, VKLL, and MKLL all within 1–2 kcal/mol of the best sequence. Notice that the MKLL:Sdc1

affinity is known experimentally, and is within 0.1 kcal/mol of the wildtype value [30]. Experimentally, the wildtype and mutant sequences have similar stabilities and the same binding affinity for Caspr4, suggesting that both should be sampled. Instead, neither one is sampled; the closest homolog is IEAV (similar to MEFV), at +2 kcal/mol (relative to the best sequence). This is probably due to steric conflict between position 915 (L or F) and the Caspr4 Phe0 in this backbone geometry.

Using the mutant backbone structure (4NXQ) and in the apo state, the room temperature Monte Carlo replica recovers the mutant MEFV at +5 kcal/mol and the wildtype LKLL at +7 kcal/mol. Both protein variants are stable experimentally; a slightly higher energy to produce LKLL seems reasonable, reflecting the energy to deform the wildtype backbone into the mutant conformation in presence of the wildtype sequence. With the Sdc1 ligand, MEFV appears at +6 kcal/mol while the close wildtype homolog IKLV is the best sequence overall and VKVL is just 3 kcal/mol higher. With the Caspr4 ligand, the mutant sequence appears at +7 kcal/mol; its homologs MQMV and MEMV appear at +5 kcal/mol; the wildtype LKLL and its close homologs do not appear, and MAFI is the second best sequence overall.

A more detailed comparison is possible with the binding affinities of the experimentally characterized mutants [30]. The experiments show that (1) affinity changes associated with each position are roughly independent of the other positions (coupling free energies of 0.4 kcal/mol or less between positions); (2) homologous changes to Leu911, Leu915, and Val920 have a very small effect on the affinity; (3) changing Lys912 to Glu reduces binding by about 0.5–1 kcal/mol (for both peptides, probably due to lost interactions with the Lys methylenes); (4) changing Leu920 to Phe affects binding differently depending on the 912 type and the peptide. These properties are mostly reproduced by our simulations. With the wildtype backbone model, considering sequences of the form NKNN (where N ∈ {I,L,V,M}), the mean apo and Sdc1-bound energies are 0.9 ± 0.6 and 1.1 ± 0.5 kcal/mol, respectively, for a mean affinity of 0.2 ± 0.8 kcal/mol (relative to IKLL, taken as a reference): mutations within the ILVM class change the Sdc1 affinity very little, consistent with experiment. We predict that NKNN → NENN mutations lead to affinity changes of +0.75 kcal/mol for both peptides, compared to 0.94 kcal/mol (Sdc1) and 0.55 kcal/mol (Caspr4) experimentally. We predict that NKNN → NKFN mutations reduce the affinity by 0.5 kcal/mol for both peptides, compared to 1.2 and 0.8 kcal/mol experimentally. Only for NENN → NEFN mutations do we see larger errors: we predict a 0.5 kcal/mol affinity loss for Sdc1 (no loss experimentally) and a 0.9 kcal/mol loss for

Caspr4 (0.5 kcal/mol *gain* experimentally. Specificity changes are predicted to be small, in qualitative agreement with experiment. For example the MKFV → MEFV mutation favors Caspr4, relative to Sdc1, by 0.2 kcal/mol, compared to 0.5 kcal/mol experimentally for the LKLL → LELL mutation.

The simulations also give information on the correlations between the four mutating positions, illustrated by covariance plots between positions 911 and 912 in Fig. 9. We see that position 911 is more diverse in the apo than the holo state, while 912 is not very sensitive to the peptide. The predicted pairwise correlations between all four protein positions are weak, so that the covariance plots mostly exhibit horizontal and vertical lines or bands, without noticeable “diagonal” structure. This agrees with the experimental affinities of the single, double, and quadruple mutants, where the affinity changes associated with each point mutation are roughly independent of the other positions [30].

5 Discussion

We have examined several parameterizations of a simple CPD model for PDZ design, implemented in the Proteus software. We tested two sets of atomic surface energy parameters and two protein dielectric values, and we optimized the amino acid chemical potentials, or reference energies for each case. We introduced a more refined description of the unfolded state than previously, where burial of each position in the folded state is taken into account, where experimental homologs are carefully chosen to define protein composition, and where the reference energy optimization has a clear statistical basis. For the folded state, we use a high quality protein force field and Generalized Born solvent model. The rotamer approximation is alleviated through a short minimization of sidechain pairs during the energy matrix calculation. The energy function and rotamer description have been extensively tested in the past for protein-ligand design [? ?]. They gave very good performance for sidechain reconstruction tests (comparable to the popular Scwrl4 program [?]) [47] and respectable performance for a large set of protein acid/base constants (superior to the Rosetta software [?], despite extensive parameter tuning) [?]. We also benefit from an effective and efficient Replica Exchange Monte Carlo sampling method, using over a half billion steps per simulation (per replica) [50]. Encouragingly, performance levels were fairly robust across model parameterizations.

The model has several limitations, most of which are widespread in CPD implementations and applications. One is the use of a fixed protein backbone. For whole protein

design, this is partly counterbalanced by the use of two or more PDZ structures to design; for example, pooling the designed Tiam1 and Cask sequences gives a mean sequence entropy comparable to the experimental Pfam set. A second limitation is the discrete rotamer approximation, which requires some adaptation of the energy function to avoid exaggerated steric clashes; the method used here is the pairwise minimization method mentioned above [26?]. A third limitation is the use of a pairwise additive energy function, which has the form of a sum over pairs of residues. In particular, the dielectric environment of each pair is assumed to be native-like. Nevertheless, the method gave good results in a large acid/base benchmark, which are very sensitive to the electrostatic treatment [?]. A fourth limitation of our model is the need, for optimal results, to parameterize the reference energies specifically for a given set of proteins. However, this step is well-automated and highly parallel. A fifth limitation is the use of protein stability as the sole design criterion, without explicitly accounting for fold specificity, protection against aggregation, functional considerations like ligand binding, or binding of other domains within the PDZ protein itself. We note, however, that the Superfamily tests did not lead to any fold misassignments (sequences that prefer another SCOP fold), and functional criteria can be introduced in an *ad hoc* way; for example the sequences tested by MD were designed with their peptide binding residues not allowed to mutate.

Designed sequences were extensively compared to experiment, through fold recognition tests, similarity calculations, and entropy calculations. Sequences were also compared to ones designed with the Rosetta software (and default parameters), which has itself been extensively tested. Similarity to Pfam sequences was mostly comparable to the similarity between the Pfam sequences themselves. For the specificity positions in Tiam1, comparison to experimental affinities was possible for some cases, yielding free energy errors on the order one 1 kcal/mol in most cases. Another attractive route for testing is through high level MD simulations and free energy calculations. Here, a handful of designed sequences were also tested in rather long MD simulations, suggesting that two (of ten simulated) are stable over 250–500 ns timescales, if not longer (despite the weak wildtype stability). Direct experimental testing of our designed sequences remains to be done, either for the full protein designs or for the Tiam1 specificity positions.

The model was used for two applications. Hydrophobic “titration” of two PDZ domains illustrates a novel way to characterize protein designability and yields a hydrophobic susceptibility (number of type changes per kcal/mol per position), which differs by a factor of two between Tiam1 and 2BYG. Redesign of four specificity positions in Tiam1

was used to test the design model, revealing some of the limitations of fixed backbone design, but also giving semi-quantitative agreement with available binding free energies. This agreement suggests that some of the new, predicted mutations could be of interest and provide new specificity properties, which remain to be studied further and tested experimentally.

Our model is mostly physics-based, although the reference energies and some parameterization aspects are empirical. Thus, it has a certain transferability to a range of molecule types, such as RNA and nonnatural amino acids (considered in an earlier protein-ligand design study [?]). It can benefit rapidly from ongoing improvements in protein force fields and solvation models. Thus, we have implemented an improved model for hydrophobic solvation, which is faster and more accurate than our current surface area energy term (manuscript in preparation). A main approximation in our solvation model (and most CPD variants) is the use of a pairwise-additive approximation of the full energy function. This approximation can now be removed in principle, thanks to a recent implementation (manuscript in preparation) of a more exact Generalized Born calculation, with an efficiency not much reduced compared to the pairwise approximation [?]. Although our unfolded model is more refined here than previously, single-position design of Tiam1 showed evidence of some systematic error, so that further work is needed. For applications to ligand binding, it is possible to upweight the protein-ligand interaction in the energy function.

In terms of sequence and conformational sampling, several improvements could be introduced in future work. While REMC is a powerful sampling method, there are cases where the global energy minimum state is required; for this, aggressive heuristic optimization approaches exist or are under development that can be applied to full protein design. We also illustrated the use of a bias potential to explore a particular region of sequence space (the Pfam vicinity). Multibackbone design is also possible with Proteus, thanks to a novel, non-heuristic hybrid Monte Carlo method that preserves Boltzmann sampling [?]. Hybrid Monte Carlo can also be extended to the problem of designing ligand binding specificity, as in the Tiam1:peptide problem above.

Acknowledgements

We are grateful for many helpful discussions with Ernesto Fuentes and Michael Schnieders (University of Iowa).

References

- [1] HARRIS, B. Z., AND LIM, W. A. Mechanism and role of PDZ domains in signaling complex assembly. *J. Cell Sci.* 114 (2001), 3219–3231.
- [2] HUNG, A. Y., AND SHENG, M. PDZ domains: Structural modules for protein complex assembly. *J. Biol. Chem.* 277 (2002), 5699–5702.
- [3] TONIKIAN, R., ZHANG, Y. N., SAZINSKY, S. L., CURRELL, B., YEH, J. H., REVA, B., HELD, H. A., APPLETON, B. A., EVANGELISTA, M., WU, Y., XIN, X. F., CHAN, A. C., SESAGIRI, S., LASKY, L. A., SANDER, C., BOONE, C., BADER, G. D., AND SIDHU, S. S. A specificity map for the PDZ domain family. *PLoS Biology* 6 (2008), 2043–2059.
- [4] GFELLER, D., BUTTY, F., WIERZBICKA, M., VERSCHUEREN, E., VANHEE, P., HUANG, H., ERNST, A., DARAND, N., STAGLJAR, I., SERRANO, L., SIDHU, S. S., BADER, G. D., , AND KIM, P. M. The multiple-specificity landscape of modular peptide recognition domains. *Molec. Syst. Biol.* 7 (2011), 484.
- [5] SUBBAIAH, V. K., KRANJEC, C., THOMAS, M., AND BAN, L. Structural and thermodynamic analysis of PDZ-ligand interactions. *Biochem. J.* 439 (2011), 195–205.
- [6] SHEPHERD, T. R., AND FUENTES, E. J. Structural and thermodynamic analysis of PDZ-ligand interactions. *Methods in Enzymology* 488 (2011), 81–100.
- [7] BACHA, A., CLAUSEN, B. H., MOLLER, M., VESTERGAARD, B., CHIC, C. N., ROUND, A., SØRENSEN, P. L., NISSEN, K. B., KASTRUP, J. S., GAJHEDE, M., JEMTH, P., KRISTENSEN, A. S., LUNDSTROM, P., LAMBERTSEN, K. L., , AND STROMGAARD, K. A high-affinity, dimeric inhibitor of PSD-95 bivalently interacts with PDZ1-2 and protects against ischemic brain damage. *Proc. Natl. Acad. Sci. USA* 109 (2012), 3317–3322.
- [8] ROBERTS, K. E., CUSHING, P. R., BOISGUERIN, P., MADDEN, D. R., AND DONALD, B. R. Computational design of a PDZ domain peptide inhibitor that rescues CFTR activity. *PLoS Comp. Bio.* 8 (2012), e1002477.
- [9] ZHENG, F., JEWELL, H., FITZPATRICK, J., ZHANG, J., MIERKE, D. F., AND GRIGORYAN, G. Computational design of selective peptides to discriminate between similar PDZ domains in an oncogenic pathway. *J. Mol. Biol.* 427 (2015), 491–510.
- [10] SOCOLICH, M., LOCKLESS, S. W., RUSS, W. P., LEE, H., GARDNER, K. H., AND RANGANATHAN, R. Evolutionary information for specifying a protein fold. *Nature* 437 (2005), 512–518.

- [11] KONG, Y., AND KARPLUS, M. Signaling pathways of PDZ2 domain: A molecular dynamics interaction correlation analysis. *Proteins* 74 (2009), 145–154.
- [12] MC LAUGHLIN JR, R. N., POELWIJK, F. J., RAMAN, A., GOSAL, W. S., AND RANGANATHAN, R. The spatial architecture of protein function and adaptation. *Nature* 458 (2012), 859–864.
- [13] MELERO, C., OLLIKAINEN, N., HARWOOD, I., KARPIAK, J., AND KORTEMME, T. Quantification of the transferability of a designed protein specificity switch reveals extensive epistasis in molecular recognition. *Proc. Natl. Acad. Sci. USA* 111 (2014), 15426–15431.
- [14] REINA, J., LACROIX, E., HOBSON, S. D., FERNANDEZ-BALLESTER, G., RYBIN, V., SCHWAB, M. S., SERRANO, L., AND GONZALEZ, C. Computer-aided design of a PDZ domain to recognize new target sequences. *Nat. Struct. Mol. Biol.* 9 (2002), 621–627.
- [15] SCHMIDT AM BUSCH, M., SEDANO, A., AND SIMONSON, T. Computational protein design: validation and possible relevance as a tool for homology searching and fold recognition. *PLoS One* 5(5) (2010), e10410.
- [16] SMITH, C. A., AND KORTEMME, T. Structure-based prediction of the peptide sequence space recognized by natural and synthetic PDZ domains. *J. Mol. Biol.* 402 (2010), 460–474.
- [17] BUTTERFOSS, G. L., AND KUHLMAN, B. Computer-based design of novel protein structures. *Ann. Rev. Biophys. Biomolec. Struct.* 35 (2006), 49–65.
- [18] LIPPOW, S. M., AND TIDOR, B. Progress in computational protein design. *Curr. Opin. Biotech.* 18 (2007), 305–311.
- [19] DAI, L., YANG, Y., KIM, H. R., AND ZHOU, Y. Improving computational protein design by using structure-derived sequence profile. *Proteins* 78 (2010), 2338–2348.
- [20] FELDMEIER, K., AND HOECKER, B. Computational protein design of ligand binding and catalysis. *Curr. Opin. Chem. Biol.* 17 (2013), 929–933.
- [21] TINBERG, C. E., KHARE, S. D., DOU, J., DOYLE, L., NELSON, J. W., SCHENA, A., JANKOWSKI, W., KALODIMOS, C. G., JOHNSSON, K., STODDARD, B. L., AND BAKER, D. Computational design of ligand-binding proteins with high affinity and selectivity. *Nature* 501 (2013), 212–218.
- [22] AU, L., AND GREEN, D. F. Direct calculation of protein fitness landscapes through computational protein design. *Biophys. J.* 110 (2016), 75–84.

- [23] POKALA, N., AND HANDEL, T. Energy functions for protein design I: Efficient and accurate continuum electrostatics and solvation. *Prot. Sci.* 13 (2004), 925–936.
- [24] SAMISH, I., MACDERMAID, C. M., PEREZ-AGUILAR, J. M., AND SAVEN, J. G. Theoretical and computational protein design. *Ann. Rev. Phys. Chem.* 62 (2011), 129—149.
- [25] LI, Z., YANG, Y., ZHAN, J., DAI, L., AND ZHOU, Y. Energy functions in de novo protein design: Current challenges and future prospects. *Ann. Rev. Biochem.* 42 (2013), 315–335.
- [26] SCHMIDT AM BUSCH, M., LOPES, A., MIGNON, D., AND SIMONSON, T. Computational protein design: software implementation, parameter optimization, and performance of a simple model. *J. Comput. Chem.* 29 (2008), 1092–1102.
- [27] SIMONSON, T. Protein:ligand recognition: simple models for electrostatic effects. *Curr. Pharma. Design* 19 (2013), 4241–4256.
- [28] POLYDORIDES, S., MICHAEL, E., MIGNON, D., DRUART, K., ARCHONTIS, G., AND SIMONSON, T. Proteus and the design of ligand binding sites. In *Methods in Molecular Biology: Design and Creation of Protein Ligand Binding Proteins*, B. Stoddard, Ed., vol. 1414. Springer Verlag, New York, 2016, p. 0000.
- [29] BAKER, D. Prediction and design of macromolecular structures and interactions. *Phil. Trans. R. Soc. Lond.* 361 (2006), 459–463.
- [30] SHEPHERD, T. R., HARD, R. L., MURRAY, A. M., PEI, D., AND FUENTES, E. J. Distinct ligand specificity of the Tiam1 and Tiam2 PDZ domains. *Biochemistry* 50 (2011), 1296–1308.
- [31] FRENKEL, D., AND SMIT, B. *Understanding molecular simulation, Chapter 3*. Academic Press, New York, 1996.
- [32] GRIMMETT, G. R., AND STIRZAKER, D. R. *Probability and random processes*. Oxford University Press, 2001.
- [33] KLEINMAN, C. L., RODRIGUE, N., BONNARD, C., PHILIPPE, H., AND LARTILLOT, N. A maximum likelihood framework for protein design. *BMC Bioinf.* 7 (2006), Art. 326.
- [34] FOWLER, R. H., AND GUGGENHEIM, E. A. *Statistical Thermodynamics*. Cambridge University Press, 1939.

- [35] CORNELL, W., CIEPLAK, P., BAYLY, C., GOULD, I., MERZ, K., FERGUSON, D., SPELLMEYER, D., FOX, T., CALDWELL, J., AND KOLLMAN, P. A second generation force field for the simulation of proteins, nucleic acids, and organic molecules. *J. Am. Chem. Soc.* **117** (1995), 5179–5197.
- [36] HAWKINS, G. D., CRAMER, C., AND TRUHLAR, D. Pairwise descreening of solute charges from a dielectric medium. *Chem. Phys. Lett.* **246** (1995), 122–129.
- [37] LOUPES, A., ALEKSANDROV, A., BATHELT, C., ARCHONTIS, G., AND SIMONSON, T. Computational sidechain placement and protein mutagenesis with implicit solvent models. *Proteins* **67** (2007), 853–867.
- [38] LEE, B., AND RICHARDS, F. The interpretation of protein structures: estimation of static accessibility. *J. Mol. Biol.* **55** (1971), 379–400.
- [39] BRÜNGER, A. T. X-PLOR version 3.1, *A System for X-ray crystallography and NMR*. Yale University Press, New Haven, 1992.
- [40] GAILLARD, T., AND SIMONSON, T. Pairwise decomposition of an MMGBSA energy function for computational protein design. *J. Comput. Chem.* **35** (2014), 1371–1387.
- [41] STREET, A. G., AND MAYO, S. Pairwise calculation of protein solvent-accessible surface areas. *Folding and Design* **3** (1998), 253–258.
- [42] ALEKSANDROV, A., POLYDORIDES, S., ARCHONTIS, G., AND SIMONSON, T. Predicting the acid/base behavior of proteins: A constant-pH Monte Carlo approach with Generalized Born solvent. *J. Phys. Chem. B* **114** (2010), 10634–10648.
- [43] SCHMIDT AM BUSCH, M., MIGNON, D., AND SIMONSON, T. Computational protein design as a tool for fold recognition. *Proteins* **77** (2009), 139–158.
- [44] ESWAR, N., MARTI-RENOM, M. A., WEBB, B., MADHUSUDHAN, M. S., ERAMIAN, D., SHEN, M., PIEPER, U., AND SALI, A. Comparative protein structure modeling with MODELLER. *Curr. Prot. Bioinf. Suppl.* **15** (2006), 5.6.1–5.6.30.
- [45] TUFFERY, P., ETCHEBEST, C., HAZOUT, S., AND LAVERY, R. A new approach to the rapid determination of protein side chain conformations. *J. Biomol. Struct. Dyn.* **8** (1991), 1267.
- [46] KRIVOV, G. G., SHAPALOV, M. V., AND DUNBRACK, R. L. Improved prediction of protein side-chain conformations with SCWRL4. *Proteins* **77** (2009), 778–795.

- [47] GAILLARD, T., PANEL, N., AND SIMONSON, T. Protein sidechain conformation predictions with an MMGBSA energy function. *Proteins* 84 (2016), 803–819.
- [48] KOFKE, D. A. On the acceptance probability of replica-exchange Monte Carlo trials. *J. Chem. Phys.* 117 (2002), 6911–6914.
- [49] EARL, D., AND DEEM, M. W. Parallel tempering: theory, applications, and new perspectives. *Phys. Chem. Chem. Phys.* 7 (2005), 3910–3916.
- [50] MIGNON, D., AND SIMONSON, T. Comparing three stochastic search algorithms for computational protein design: Monte Carlo, Replica Exchange Monte Carlo, and a multistart, steepest-descent heuristic. *J. Comput. Chem.* 37 (2016), 1781–1793.
- [51] GOUGH, J., KARPLUS, K., HUGHEY, R., AND CHOTHIA, C. Assignment of homology to genome sequences using a library of hidden Markov models that represent all proteins of known structure. *J. Mol. Biol.* 313 (2001), 903–919.
- [52] WILSON, D., MADERA, M., VOGEL, C., CHOTHIA, C., AND GOUGH, J. The SUPERFAMILY database in 2007: families and functions. *Nucl. Acids Res.* 35 (2007), D308–D313.
- [53] ANDREEVA, A., HOWORTH, D., BRENNER, S. E., HUBBARD, J. J., CHOTHIA, C., AND MURZIN, A. G. SCOP database in 2004: refinements integrate structure and sequence family data. *Nucl. Acids Res.* 32 (2004), D226–229.
- [54] DURBIN, R., EDDY, S. R., KROGH, A., AND MITCHISON, G. *Biological sequence analysis*. Cambridge University Press, 2002.
- [55] MURPHY, L. R., WALLQVIST, A., AND LEVY, R. M. Simplified amino acid alphabets for protein fold recognition and implications for folding. *Prot. Eng.* 13 (2000), 149–152.
- [56] LAUNAY, G., MENDEZ, R., WODAK, S. J., AND SIMONSON, T. Recognizing protein-protein interfaces with empirical potentials and reduced amino acid alphabets. *BMC Bioinf.* 8 (2007), 270–291.
- [57] JO, S., KIM, T., IYER, V. G., AND IM, W. CHARMM-GUI: a web-based graphical user interface for CHARMM. *J. Comput. Chem.* 29 (2008), 1859–1865.
- [58] DARDEN, T. Treatment of long-range forces and potential. In *Computational Biochemistry & Biophysics*, O. Becker, A. Mackerell Jr., B. Roux, and M. Watanabe, Eds. Marcel Dekker, N.Y., 2001, ch. 4.

- [59] JORGENSEN, W., CHANDRASEKAR, J., MADURA, J., IMPEY, R., AND KLEIN, M. Comparison of simple potential functions for simulating liquid water. *J. Chem. Phys.* **79** (1983), 926–935.
- [60] BROOKS, B., BROOKS III, C. L., MACKERELL JR., A. D., NILSSON, L., PETRELLA, R. J., ROUX, B., WON, Y., ARCHONTIS, G., BARTELS, C., BORESCH, S., CAFLISCH, A., CAVES, L., CUI, Q., DINNER, A. R., FEIG, M., FISCHER, S., GAO, J., HODOSCEK, M., IM, W., KUCZERA, K., LAZARIDIS, T., MA, J., OVCHINNIKOV, V., PACI, E., PASTOR, R. W., POST, C. B., PU, J. Z., SCHAEFER, M., TIDOR, B., VENABLE, R. M., WOODCOCK, H. L., WU, X., YANG, W., YORK, D. M., AND KARPLUS, M. CHARMM: The biomolecular simulation program. *J. Comp. Chem.* **30** (2009), 1545–1614.
- [61] PHILLIPS, J. C., BRAUN, R., WANG, W., GUMBART, J., TAJKHORSHID, E., VILLA, E., CHIPOT, C., SKEEL, R. D., KALE, L., AND SCHULTEN, K. Scalable molecular dynamics with NAMD. *J. Comput. Chem.* **26** (2005), 1781–1802.
- [62] SCHMIDT AM BUSCH, M., LOPES, A., AMARA, N., BATHELT, C., AND SIMONSON, T. Testing the Coulomb/Accessible Surface Area solvent model for protein stability, ligand binding, and protein design. *BMC Bioinformatics* **9** (2008), 148–163.

Table 1: Test proteins and their homologs

PDB code	residue numbers	# active positions	number of homologs	E-value threshold	identity % range	protein acronym
1G9O	9-99	76	62	1e-32	67-95	NHERF
1IHJ	12-105	82	42	1e-10	38-95	INAD
1N7E	667-761	79	48	1e-45	84-95	GRIP
1R6J	192-273	72	85	1e-43	85-95	syntenin
2BYG	186-282	82	43	1e-41	78-95	DLG2
3K82	305-402	80	50	1e-46	81-95	PSD95
1KWA	487-568	74	126	7e-28	60-85	Cask
4GVD	837-930	84	50	2e-23	60-85	Tiam1

E-values are for the Blast search for experimental homologs. Identity % is between the homologs and the query protein. Active positions are those that can mutate during the design simulations.

Table 2: Model variants

model name	model symbol	dielectric constant	σ_i set	# target proteins	σ_i values (cal/mol/Å ²) (unpol,arom,polar,ionic)
A	($\epsilon_P=8, S1, n=6$)	8	set 1	6	-5, -12, -8, -9
A'	($\epsilon_P=8, S1, n=2$)	8	set 1	2	-5, -12, -8, -9
B	($\epsilon_P=8, S2, n=2$)	8	set 2	2	-5,-40,-80,-100
B'	($\epsilon_P=4, S2, n=2$)	4	set 2	2	-5,-40,-80,-100

n is the number of proteins whose experimental composition forms the target set; σ_i are the atom surface energy coefficients.

Table 3: Unfolded state reference energies E_t^r (kcal/mol)

Residues	Peptide ^b	Model A		Model B	
		Buried	Exposed	Buried	Exposed
ALA	0.00	0.00	0.00	0.00	0.00
CYS	-1.04	-1.04	-1.04	-0.85	-0.85
THR	-3.82	-3.82	-3.82	-5.44	-5.44
ASP	-9.17	-9.19	-9.80	-11.90	-15.88
GLU	-7.88	-7.90	-8.51	-11.97	-15.95
ASN	-5.64	-5.94	-6.00	-7.82	-10.22
GLN	-4.42	-4.72	-4.78	-7.07	-9.47
HIP ^a	15.72	14.53	14.96	12.53	9.73
HIE ^a	12.62	11.43	11.85	10.49	7.69
HID ^a	13.16	11.96	12.39	10.86	8.06
ILE	1.63	4.72	2.11	4.63	3.63
VAL	-2.25	0.83	-1.77	0.26	-0.74
LEU	-1.92	1.17	-1.44	-0.12	-1.12
LYS	-4.21	-4.56	-4.47	-6.76	-10.17
MET	-2.44	-2.78	-3.54	-2.05	-2.40
ARG	-25.30	-28.29	-28.90	-32.00	-35.18
SER	-2.85	-3.73	-2.80	-3.71	-4.74
PHE	-1.42	-0.37	-2.55	-0.23	-4.17
TRP	-2.66	-1.61	-3.79	-2.21	-6.15
TYR	-4.56	-4.20	-6.10	-5.80	-9.82

^aThe three His protonation states each have their own E_t^r values. ^bEnergies of each sidechain type within an extended peptide structure (averaged over positions and rotamers), which represents an alternate unfolded state model.

Table 4: Amino acid composition (%) of experimental and designed PDZ proteins

R	Design, model A				Experiment, n=6 set				Experiment, n=2 set				Design, model B			
	Buried		Exposed		Buried		Exposed		Buried		Exposed		Buried		Exposed	
A	11.1	17.0	4.4	12.0	10.9		4.6		5.9		4.6		4.1	12.7	7.2	13.6
C	0.0		0.3		1.3	16.9	0.5	13.4	1.5	11.2	1.2	13.4	8.6	[1.5]	5.8	[0.2]
T	5.9	[0.1]	7.3	[-1.4]	4.7		8.3		3.8		7.6		0.0	0.6		
D	4.5	6.7	5.6	16.7	4.3	6.8	6.0	17.9	3.5	9.6	6.2	16.7	7.4	9.4	8.0	16.1
E	2.2	[-0.1]	11.1	[-1.2]	2.5		11.9		6.1		10.5		2.0	[-0.2]	8.1	[-0.6]
N	2.5	4.7	7.5	14.0	2.6	4.7	6.7	12.2	1.9	2.7	7.4	16.1	1.8	2.8	8.6	17.1
Q	2.2	[0.0]	6.5	[1.8]	2.1		5.5		0.8		8.7		1.0	[0.1]	8.5	[1.0]
H ⁺	1.0		5.2		1.2		5.0		0.7		4.7		0.1	0.9	1.8	4.5
H _e	0.1	1.1	0.4	5.6	0.0	1.2	0.0	5.0	0.0	0.7	0.0	4.7	0.6	[0.2]	2.2	[-0.2]
H _δ	0.0	[-0.1]	0.0	[0.6]	0.0		0.0		0.0		0.0		0.2	0.5		
I	16.9	52.1	4.1	14.0	16.0		4.2		15.7		4.1		25.1	46.7	8.4	15.3
V	16.7	[1.4]	5.6	[0.0]	16.5	50.7	5.4	14.0	13.5	49.6	5.5	14.4	12.8	[-2.9]	3.3	[0.9]
L	18.5		4.3		18.2		4.4		20.4		4.8		8.8	3.6		
K	1.5	1.5 [-1.0]	13.0	13.0 [2.1]	2.5	2.5	10.9	10.9	6.5	6.5	10.1	10.1	5.5	5.5 [-1.0]	10.8	10.8 [0.7]
M	1.6	1.6 [0.7]	1.4	1.4 [-0.1]	0.9	0.9	1.5	1.5	5.0	5.0	1.4	1.4	5.9	5.9 [0.9]	1.4	1.4 [0.0]
R	2.5	2.5 [-0.3]	6.1	6.1 [-2.6]	2.8	2.8	8.7	8.7	1.8	1.8	9.5	9.5	2.2	2.2 [0.4]	9.1	9.1 [-0.4]
	type	class	type	class	type	class	type	class	type	class	type	class	type	class	type	class

Compositions are given for buried/exposed positions, for individual amino acid types (left) and for classes (right); values in brackets (right) are the deviations between design and experiment per class.

The $n=2$ experimental target set includes the Tiam1 and Cask homologs; the $n=6$ set includes the homologs of the other 6 test proteins. Design results are shown for models A, B.

Table 5: Fold recognition of designed sequences by Superfamily

Protein	Design model	^a Match/seq length	^b Superfamily E-value	^c Superfamily success #	^b Family E-value	^c Family success #
1G9O	A	78/91	2.5e-3	10000	3.0e-3	10000
1IHJ	A	86/94	5.6e-7	10000	2.3e-3	10000
1N7E	A	81/95	1.1e-6	10000	2.4e-3	10000
1R6J	A	41/82	1.5	1350	2.6e-2	1350
2BYG	A	77/97	1.0e-2	10000	2.3e-3	10000
3K82	A	79/97	5.8e-10	10000	3.6e-3	10000
Tiam1	A	43/94	1.3	442	4.0e-2	374
Cask	A	72/83	2.3e-4	10000	1.5e-2	10000
Tiam1	B'	53/94	1.0e-4	10000	7.0e-2	5259
Cask	B'	76/83	5.1e-7	10000	1.6e-2	10000
Tiam1	B	64/94	1.2e-4	9920	5.2e-2	9058
Cask	B	71/83	3.2e-7	10000	8.2e-3	10000
1G9O	Rosetta	79/91	1.3e-13	10000	2.2e-3	10000
1IHJ	Rosetta	85/94	7.4e-14	10000	3.7e-3	10000
1N7E	Rosetta	84/95	2.2e-10	10000	1.2e-3	10000
1R6J	Rosetta	76/82	7.3e-13	10000	1.8e-3	10000
2BYG	Rosetta	86/97	1.3e-9	10000	9.6e-4	10000
3K82	Rosetta	90/97	3.7e-23	10000	5.2e-4	10000
Tiam1	Rosetta	65/94	4.4e-4	9035	2.8e-2	9030
Cask	Rosetta	68/83	2.8e-5	9832	7.5e-3	9832

^aThe average match length for sequences recognized by Superfamily and the total sequence length.

^bAverage E-values for Superfamily assignments to the correct SCOP superfamily/family. ^cThe number of designed sequences (out of 10000 tested) assigned to the correct SCOP superfamily/family.

Table 6: Desining Tiam1 specificity positions

==
—

QM design.

Figure captions

1. **A)** 3D view of four PDZ domains. C_β 's of 14 hydrophobic core residues are shown as spheres; N- and C-termini are labelled; also three core positions designed further on (Tiam1 numbers). **B)** Cluster representation; links are annotated with backbone rms deviations (\AA) over at least 60 aligned residues (see text) and identity scores. Dashed lines correspond to more distant neighbors.
2. Alignment of experimental PDZ sequences. The top 8 are our test proteins; the others are the Pfam seed alignment, limited to its upper half for reasons of space. 14 hydrophobic core positions are indicated by red arrows; secondary structure elements are shown.
3. Sequence logos for the conserved hydrophobic core for designed and experimental Tiam1 and Cask sequences. “Exp” corresponds to the close homologs in our target set of sequences (used for E_t^r optimization); “Pfam” corresponds to the Pfam seed alignment. Proteus sequences were generated with model B. The height of each letter is proportional to the abundance of each type at the corresponding positions in the Proteus/Rosetta simulations or the experimental sequences.
4. Same as Fig. 3 for 16 surface positions (see text), Tiam1 only.
5. Histograms of Blosum40 similarity scores, relative to the Pfam RP55 sequence set, for our eight test proteins and 14 conserved hydrophobic core positions. Values are shown for Proteus (model A), Rosetta, and Pfam sequences (all compared to RP55). The similarity score of the wildtype sequence is indicated in each panel by a vertical arrow.
6. Histograms of Blosum40 similarity scores, relative to the Pfam RP55 sequence set, for Tiam1 and Cask, for all positions (top), 14 core positions (middle), and 16 surface positions (bottom). Values are shown for Proteus, Rosetta, and Pfam sequences (all compared to RP55). The similarity score of the wildtype sequence is indicated in each panel by a vertical arrow.
7. Wildtype and five designed sequences subjected to molecular dynamics simulations for 200-400 nanoseconds; backbone rms deviations are shown for each protein vs. time (in \AA ; computed for all but 7 residues at the chain termini). Right: the mean structures from the wildtype (red) and sequence-6 (blue) simulations are compared to the initial, experimental structure (gray); 20 instantaneous snapshots taken every 20 ns from the sequence-6 simulation are also shown (light, semi-transparent gray).
8. **A)** Tiam1 sequences designed with different levels of bias opposing (top) or favoring (bottom) hydrophobic types. Five low energy sequences from each simulation are shown;

the middle simulation has zero bias. Hydrophobic positions are colored according to the simulation where they appear first: from brown (top) to yellow (bottom). The 14 hydrophobic core positions are indicated by red arrows; some are numbered. **B)** 3D Tiam1 structure (stereo) with residue colors as in **A**). Only three levels of bias are shown: the two extremes and the middle (zero bias). The backbone is show in light, semi-transparent gray.

9. Design of four Tiam1 specificity positions. **A)** Xray structures (stereo) with the wildtype sequence (4GVD) or the quadruple mutant (4NXQ), with bound Sdc1 and Caspr4, respectively. The four designed sidechains are shown. **B)** Logo representation of designed sequences with no ligand (apo) or Sdc1 or Caspr4, using the wildtype (left) or mutant (right) Xray structure. **C)** Covariance plots for the 911, 912 pair: populations of each pair of types are shown as levels of color, with yellow the most highly-populated and red the lowest. Results computed with the wildtype backbone.

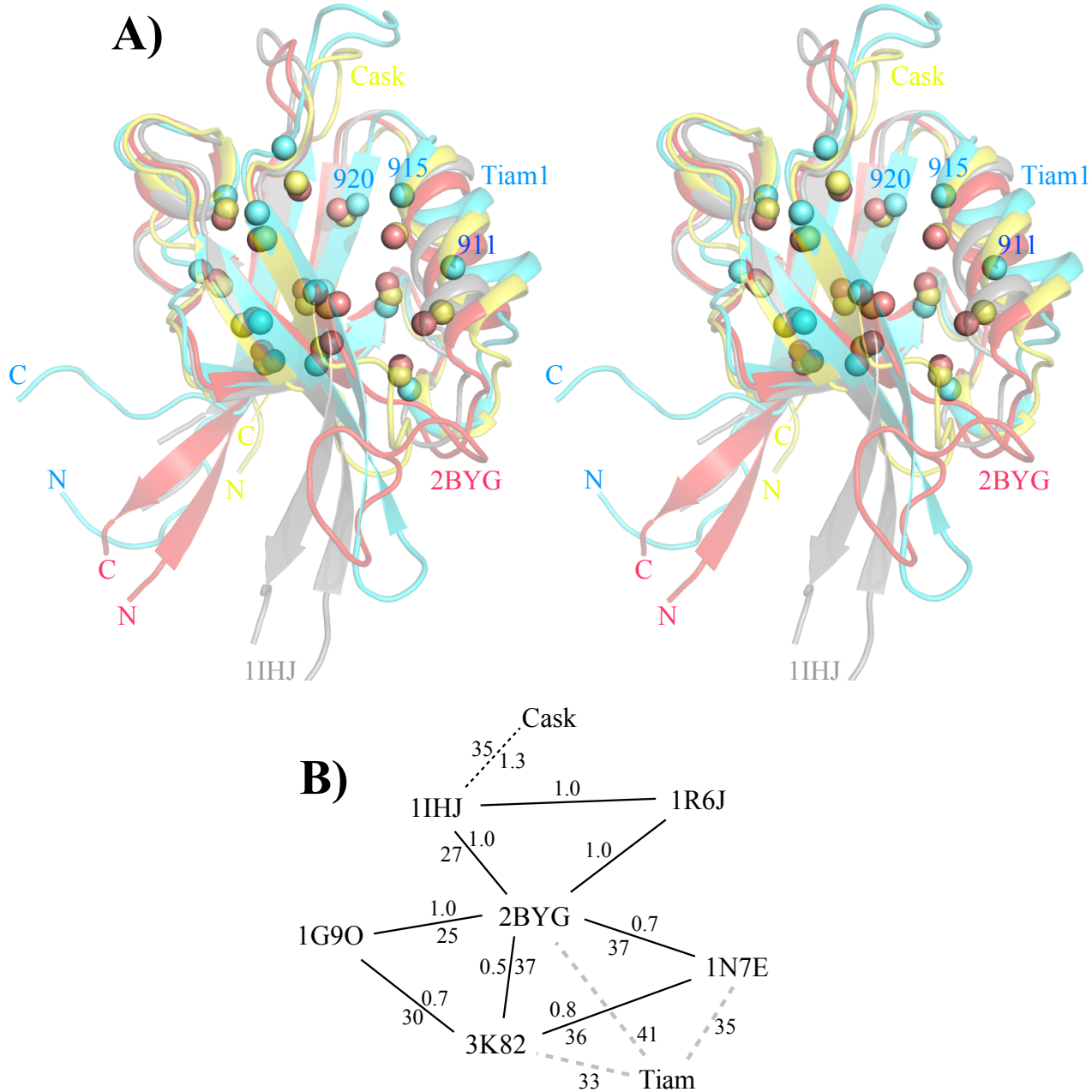


Figure 1: **A)** 3D view of four PDZ domains. **B)** Cluster representation.

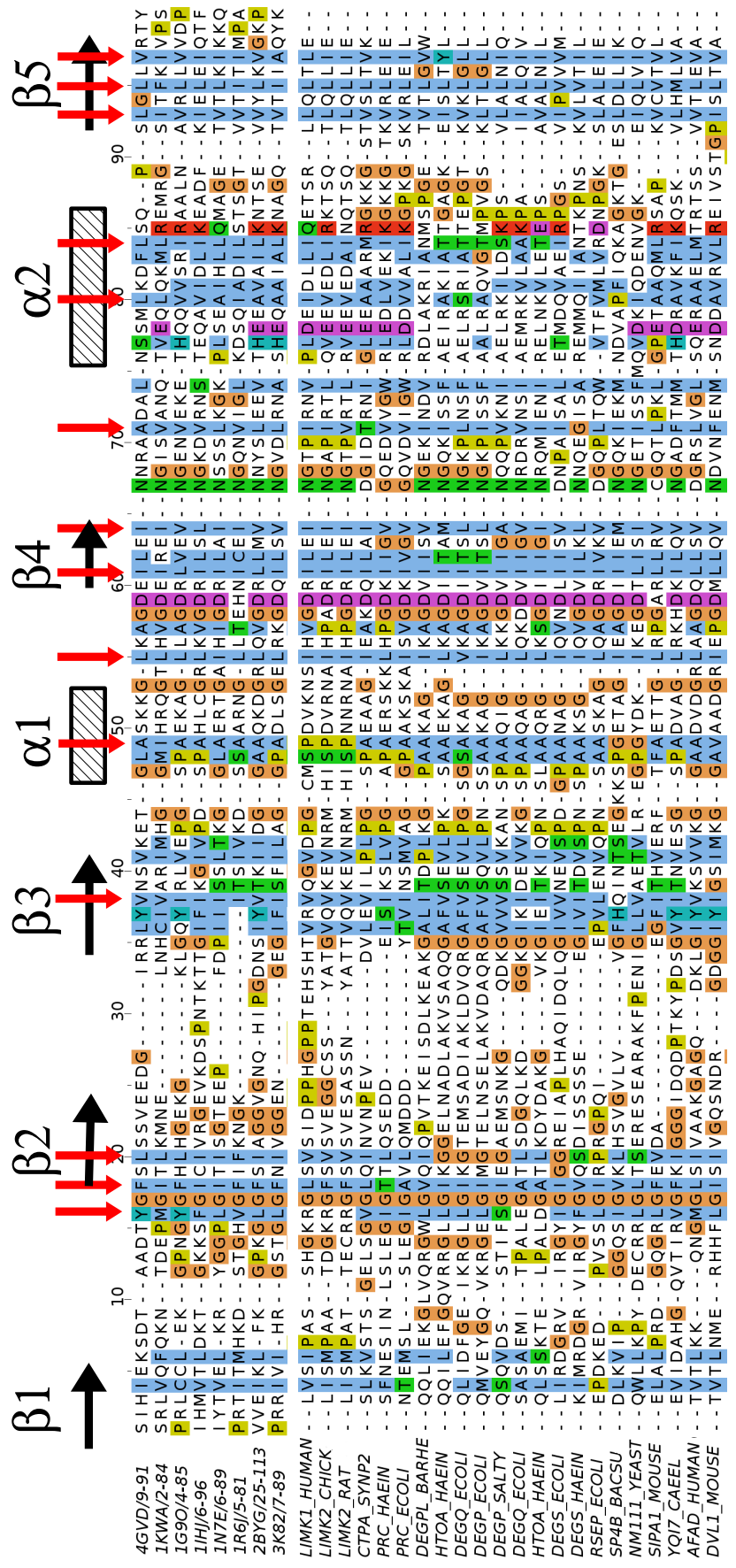


Figure 2: Alignment of experimental PDZ sequences.

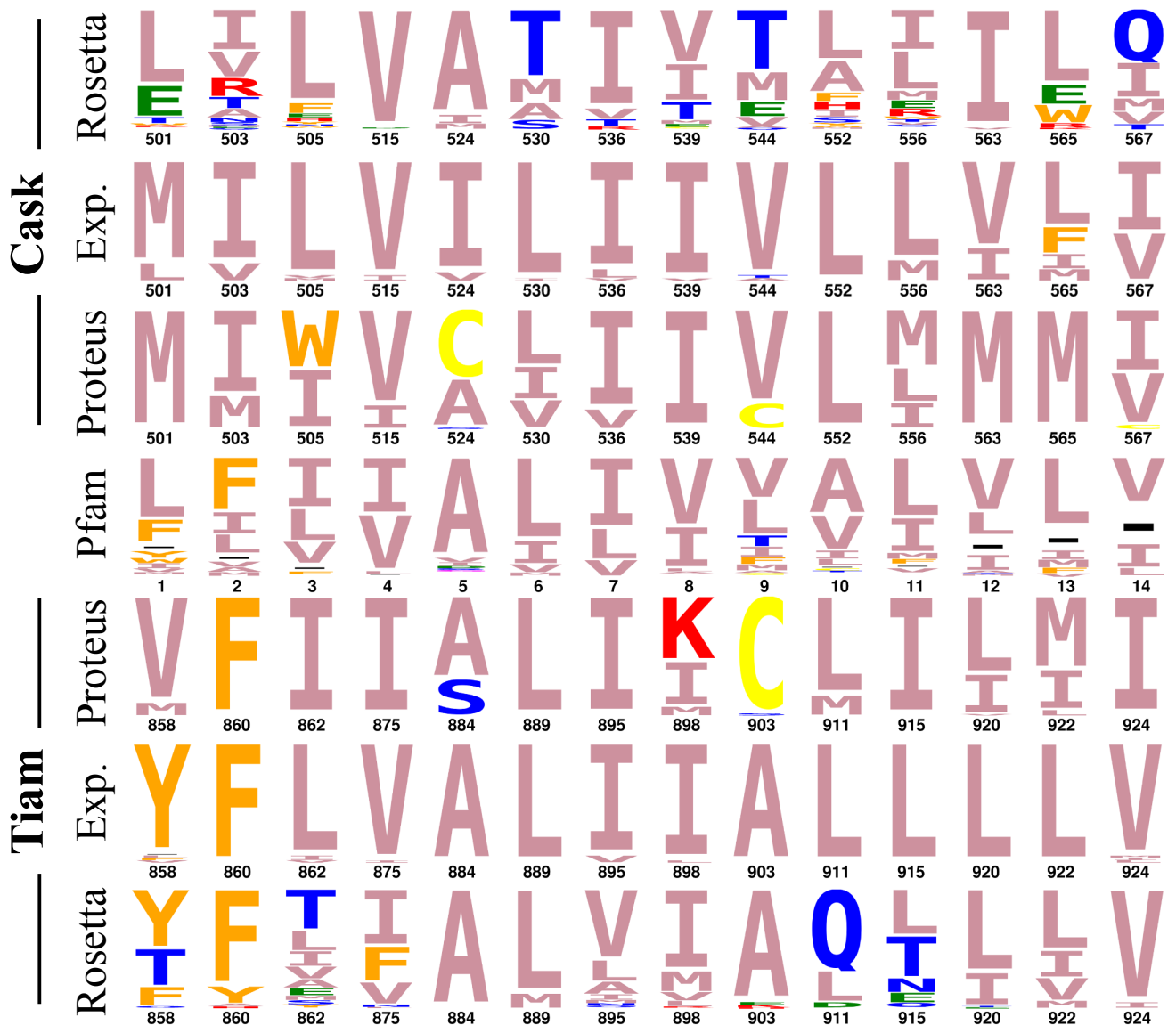


Figure 3: Core logos.



Figure 4: Surface logos.

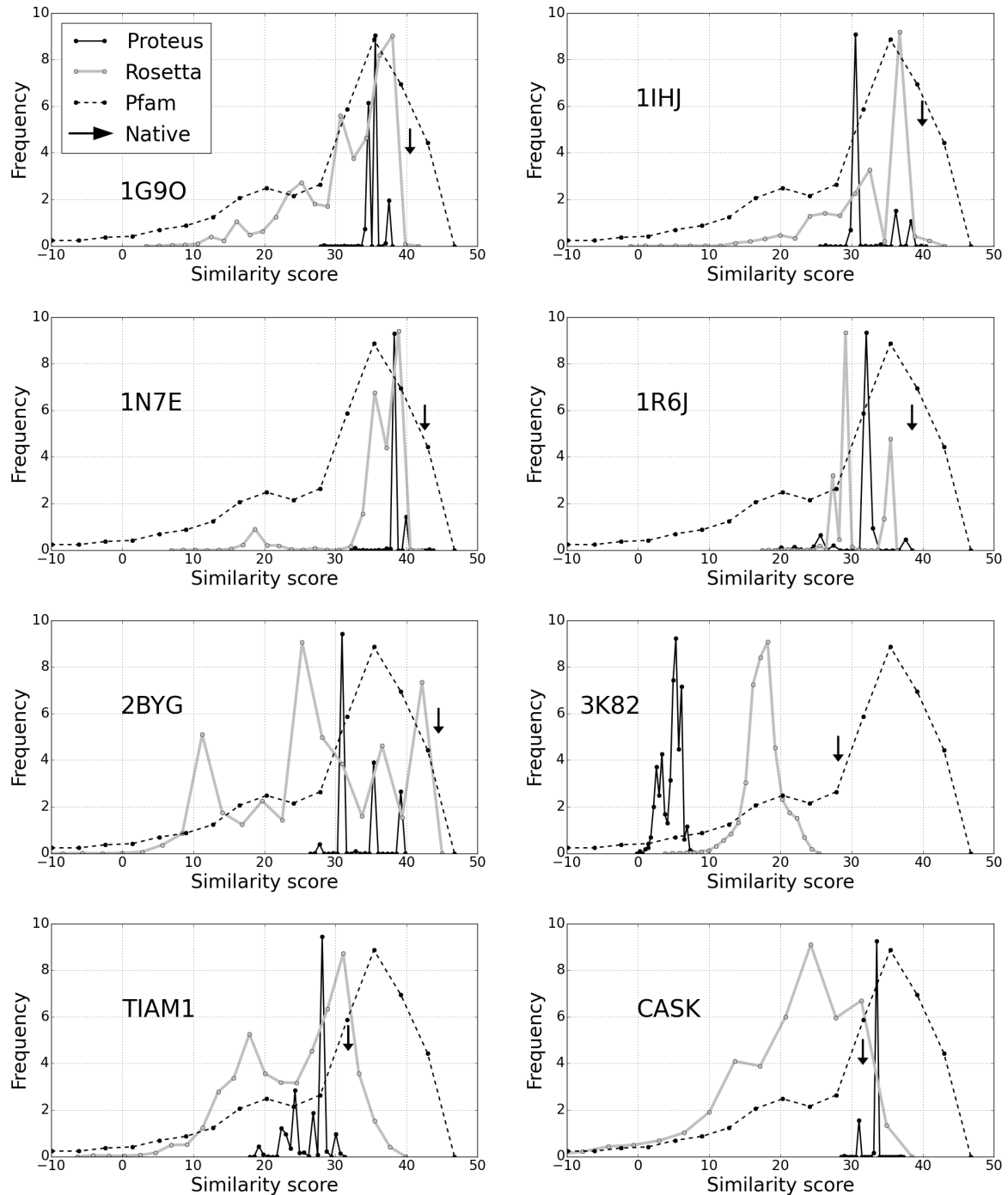


Figure 5: Similarity scores.

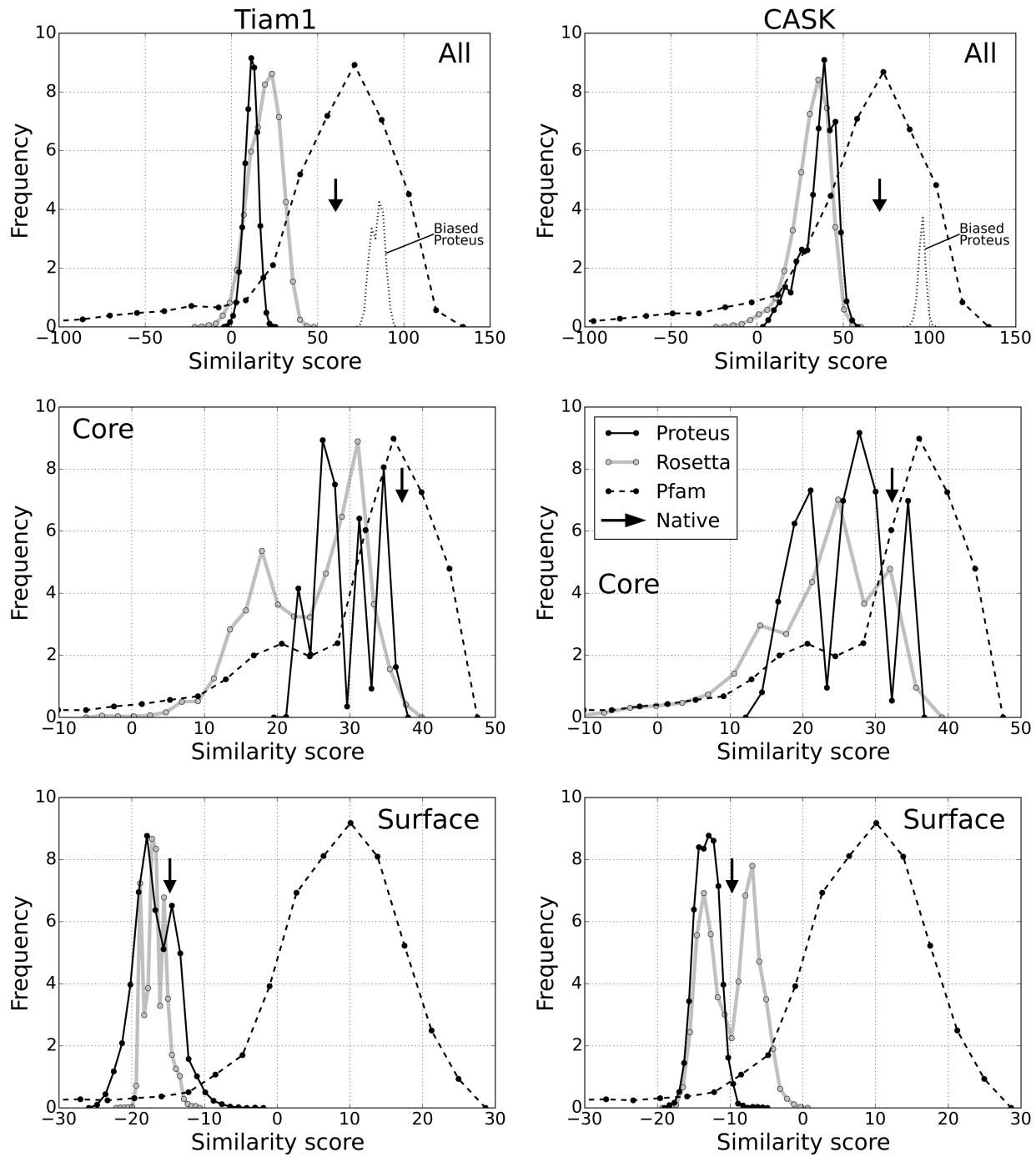


Figure 6: Similarity scores.

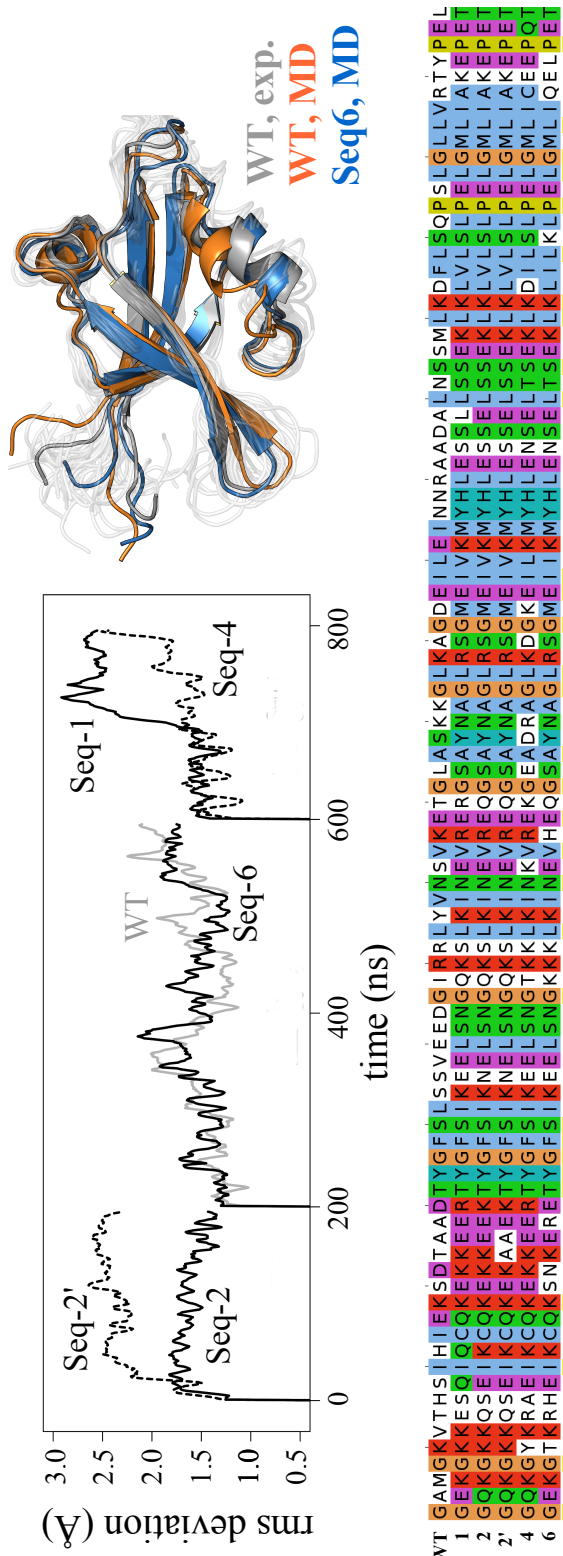


Figure 7: MD figure.

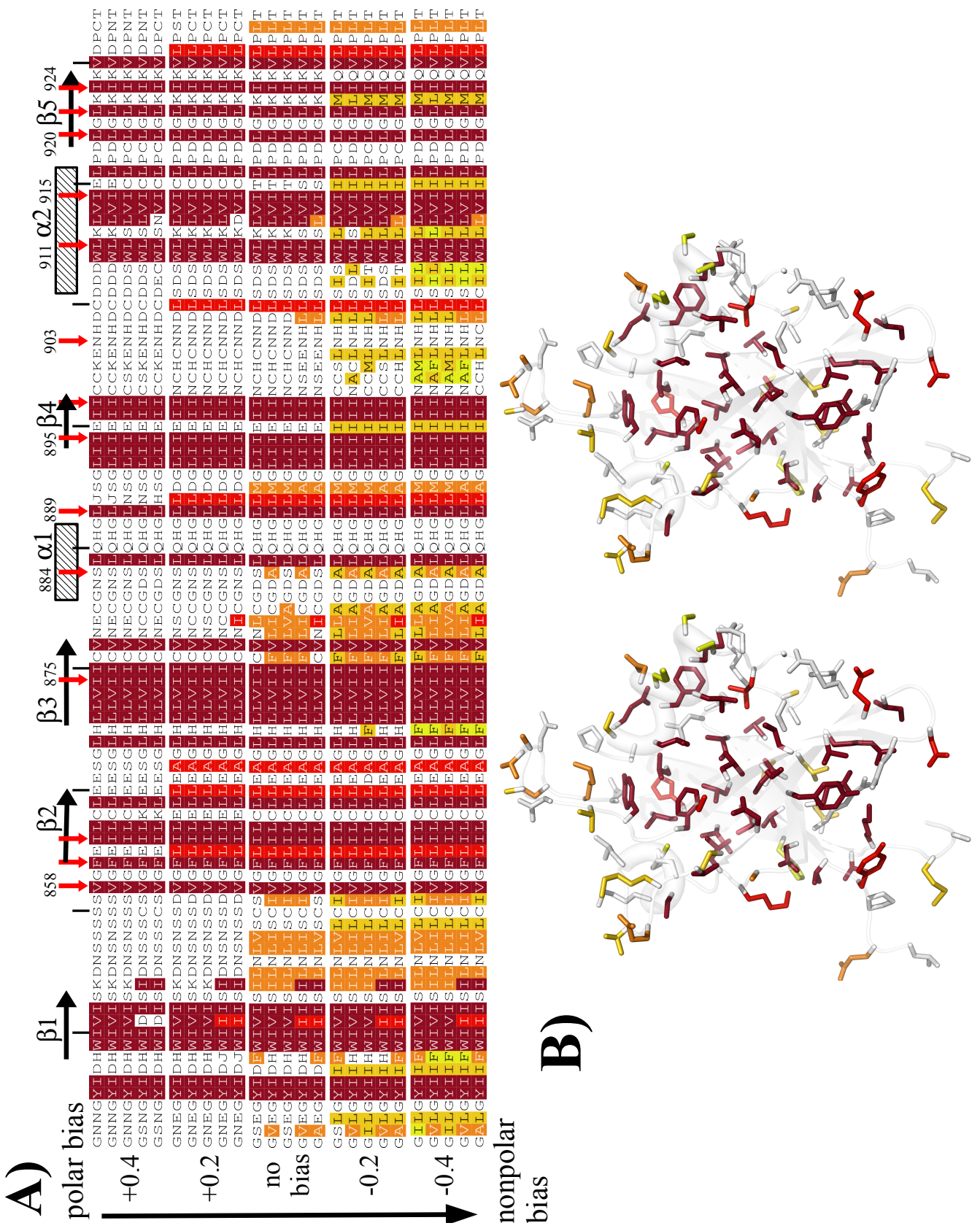


Figure 8: Hyd4phobic titration.

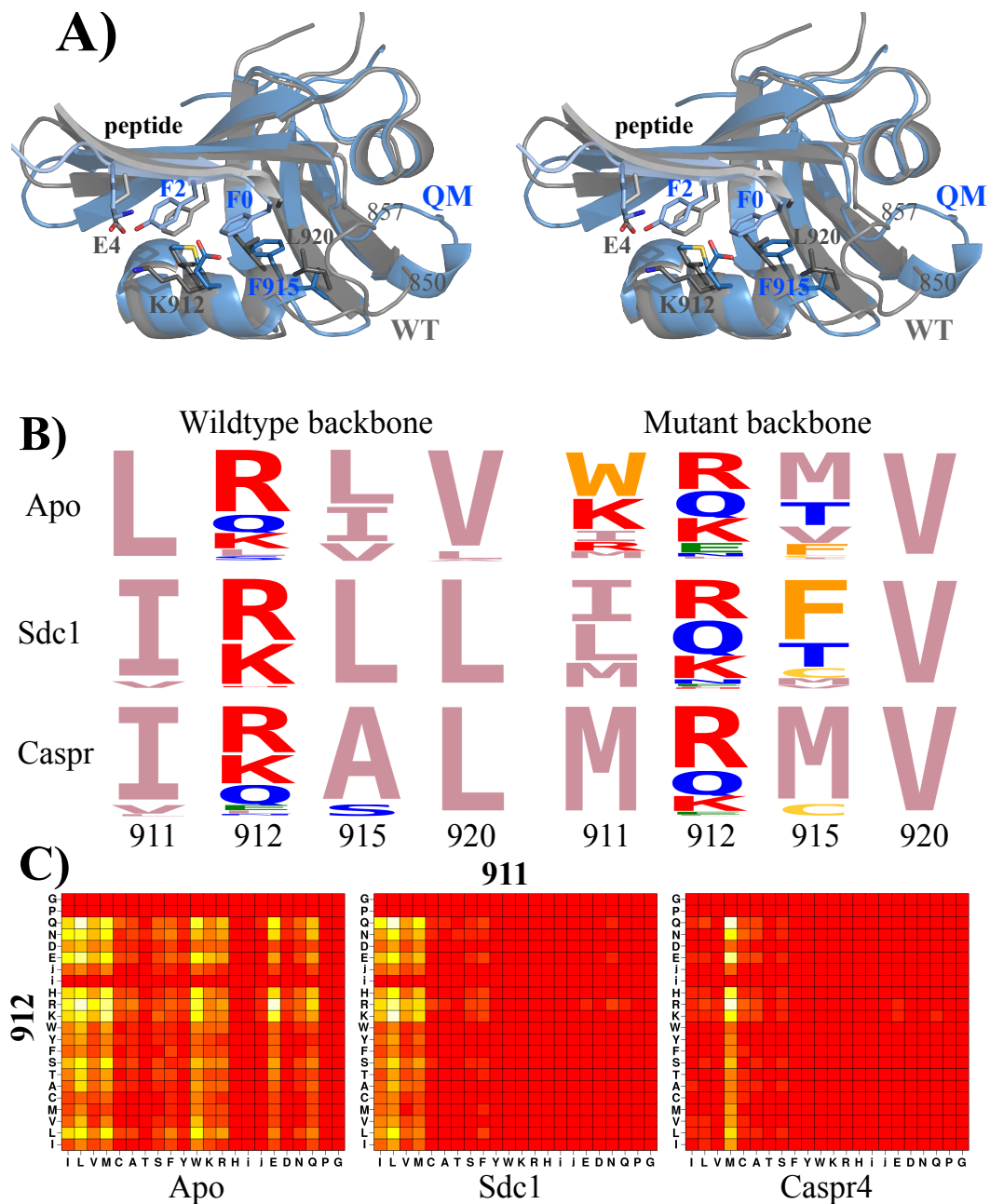


Figure 9: Quadruple mutant design.